5-2013

A geochemical investigation of Late Holocene lake sediment cores from Pyramid Lake, Fiordland, New Zealand

David J. Harning
Bates College, dharning@bates.edu

A geochemical investigation of Late Holocene lake sediment cores from Pyramid Lake, Fiordland, New Zealand

A thesis
presented to
The Faculty of Geology
Bates College
in partial fulfillment of the requirements for the
Degree of Bachelor of Science
by

David John Harning

Lewiston, Maine
April 1, 2013

Abstract

Pyramid Lake is a small, semi-closed lake thought to have formed 12000 – 13000 years ago, following the Green Lake Landslide at the end of the last glaciation. Recent records of watershed history indicate regional climate variability from natural and anthropogenic sources. Biogenic silica, stable isotopes ($\delta^{13}C$ and $\delta^{15}N$), elemental carbon and nitrogen and compound-specific lipids (n-alkanes and carboxylic acids) were examined in two sediment cores, 28 and 36 cm, collected from Pyramid Lake to shed light on organic matter sources and primary production within the lake. Carbon isotopes ranged from -27.6‰ to -28.5‰ displaying a near constant trend up core while nitrogen isotopes ranged from 0.9‰ to 1.9‰, showing a slight enrichment up core. Biogenic silica ranged from 0.97% to 23.8% and increased towards to the top of the cores. Elemental carbon and nitrogen percentages both increase mid-core with values shifting from 7 to 14 percent and 0.5 to 1 percent, respectively. Compound-specific results suggest a high proportion of vascular plants with limited algal signatures. Ages were determined via $^{239+240}$Pu-dating and range from 1855 to 1963. Results in conjunction with C/N ratios suggest possible increases in littoral sediment redistribution and/or primary productivity beginning around 1923 in association with 20th century warming. By learning how the lake's internal processes and conditions have changed in response to its environment, we can gain an understanding of the extent of human impact and predict how it could change in the future in the face of human-induced climate change.

Acknowledgments

This project would never have been accomplished if it were not for a core group of intelligent, willing and caring geologists both at Bates and abroad. First, I would like to thank Chris Moy and the University of Otago for granting me the opportunity to spend 48 wet, cold and miserable hours slogging through mountain beech forests and swamps to collect my sediment cores. The one hour the sun came out has become one of my fondest memories associated with this thesis, we all needed that. To my advisor Bev, I cannot think of anyone I would have rather worked with this past year. Your attention to my project and willingness to get deeper and deeper into laboratory procedures (which at times seemed endless) helped make this thesis. I cannot thank you enough for inspiring me to pursue my interests in environmental geology and for supporting me all these years, you are an exceptional teacher in so many ways beyond academia. Phil, your guiding in the lab will always be appreciated. Were it not for you I would still be looking at baggies of frozen sediment. To my friends and family, thanks for holding down the fort and providing me with much needed respite. To the Hoffman Fellowship and BSRF, your funding was instrumental in allowing me to pursue everything I wished to accomplish. And finally to my fellow seniors of Bates Geo, I do not know a group of students so cohesive and down to earth. From seminars to Coram to Bretton Woods and all else, it's been one hell of a ride together. Cheers to our accomplishments and the incredible adventures that await us!

Contents

List of Figures

Chapter 1: Introduction

Purpose and Significance

The sediments which continuously collect on the bottom of a lake contain a rich history in terms of the physical and chemical compositions of organic matter. Through interpretations of these proxies we are provided a record of environmental change through time. To date there has been little research conducted in Fiordland, New Zealand paleolimnology. Therefore, this project employs a multi-proxy approach to reconstruct primary productivity and sources of organic matter for Pyramid Lake through the Late Holocene using geochemical assays in an attempt to draw links between climate change and paleoenvironmental conditions. By learning how the lake's internal processes and conditions have changed in response to its environment, we can gain an understanding of the extent humans have impacted the region and may predict how it could change given time in the face of modern climate change.

Climate

Atmospheric Circulation

New Zealand consists of two islands, North Island and South Island, between 34 and 47°S latitude (Salinger and Mullan, 1999) (Figure 1.1). It is located within the Circumpolar Westerly wind belt and its relatively remote and isolated setting from other significant land masses allows the atmospheric circulation to have a profound effect on regional climate, especially on the South Island (Figure 1.2). The relative strength and position of the Circumpolar Westerlies is modulated predominantly by the Southern Annular Mode (SAM), a large-scale Southern Hemisphere climate mode responsible for redistribution of sea-level pressure (SLP) between the polar latitudes south of 60°S and the midlatitudes centered at 45°S on an inter-annual to centennial cycle (Page et al., 2010; Salinger and Mullan, 1999). Positive (negative) phases are characterized by increased (decreased) SLP gradients between the high and midlatitudes resulting in weakened (strengthened) Westerlies. Thus, over the South Island during position (negative) SAM, winds come from northeast (southwest) (Figure 1.3) (Ummenhofer et al., 2009).

The interaction of atmospheric circulation and the distinctly rugged orography of New Zealand produce heterogeneous climates over short distances throughout the country. These localized climates are strongly influenced by precipitation, which itself is modulated by changes in east-west tropospheric circulation and sea level pressures over the equatorial Pacific Ocean (Ummenhofer and England, 2007; Rump et al., 2004). The periodicity in the sea level pressure gradient shifts and subsequent climatic shifts, known as the El Niño-Southern Oscillation (ENSO), appear to be irregular occurring about every 5 years and strongly effect the oceanic circulation and delivery of warmer and cooler temperatures to New Zealand (Rump et al., 2004). ENSO oscillates between the warm oceanic phase, El Niño, associated with high SLP in the western Pacific and the cooler phase, La Niña, characterized by high SLP in the eastern Pacific Ocean (Rump et al., 2004).

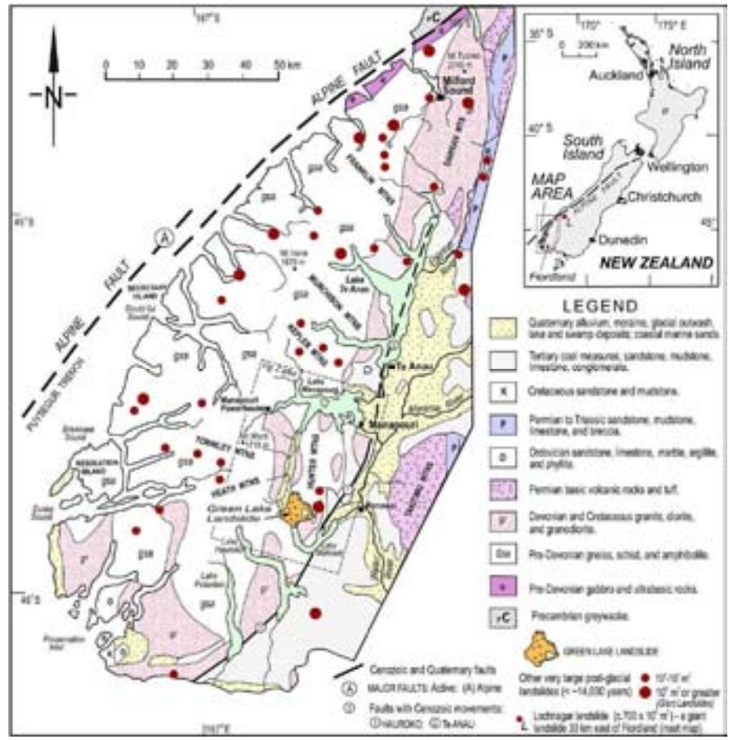

Figure 1.1: Geological map of Fiordland showing the main rock types, tectonic features, and location of Green Lake Landslide. Inset shows location of map area within New Zealand as well as the extent of the Alpine Fault. The N-S trending fault to the east of the Green Lake Landslide, where Pyramid Lake is located, denotes the Hauroko and Te Anau faults. See Figure 1.6 for Green Lake Landslide regional map, modified from Hancox and Perrin (2009).

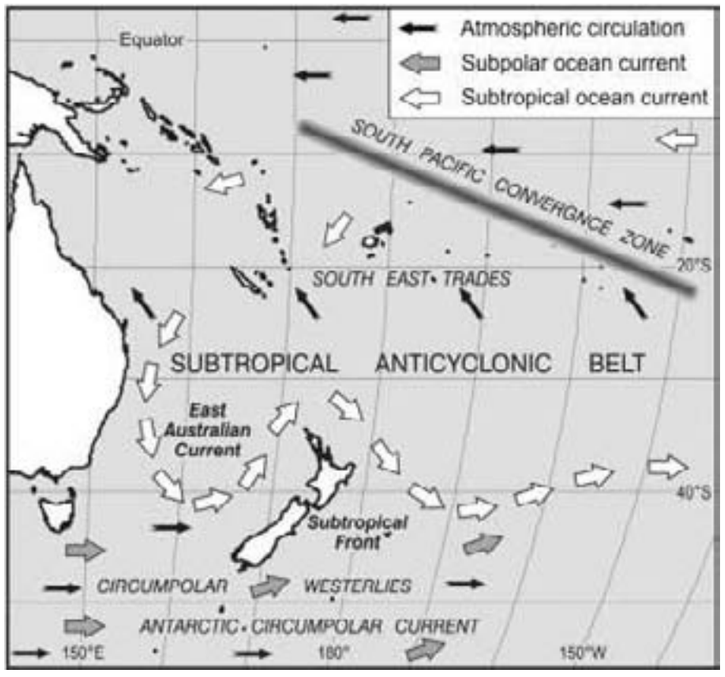

Figure 1.2: Location of New Zealand with respect to global atmospheric circulation patterns, i.e. circumpolar westerlies, and subpolar and subtropical ocean currents, from Newnham et al. (2012).

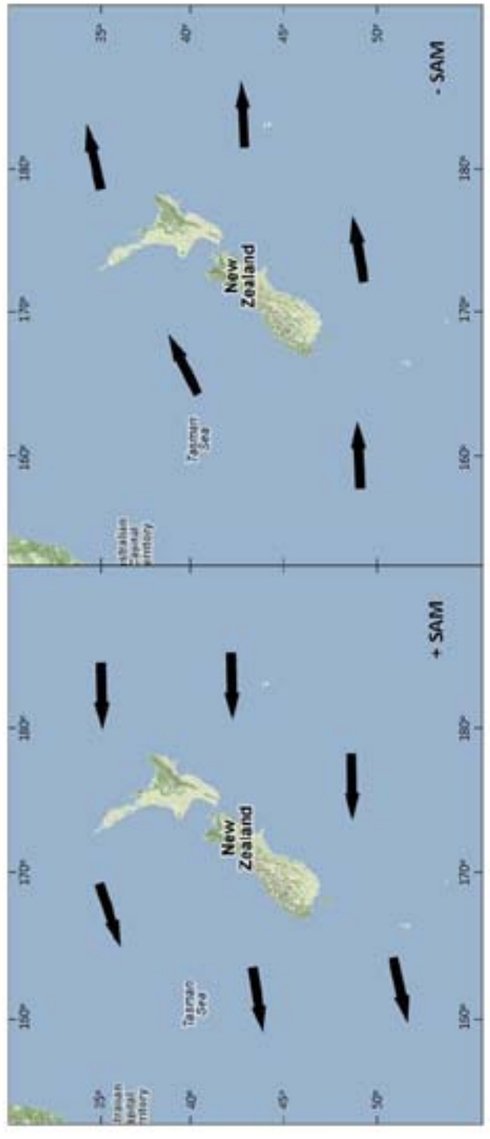

Figure 1.3: Resulting atmospheric circulation patterns and wind flow from the Southern Annular Mode (SAM). +SAM phase (left) is characterized by enhanced northeasterly airflow due to weakened westerlies and -SAM phase by enhanced westerlies (right), modified from Google Maps (2012).

Regional Precipitation Patterns

New Zealand's National Institute of Water and Atmospheric Research (NIWA) has recorded mean annual precipitation values for the Fiordland region in excess of 6000 mm yr^{-1} with measurements closer to 2500 mm yr^{-1} in the vicinity of Pyramid Lake (Hancox and Perrin, 2009; Ummenhofer and England, 2007). SAM and ENSO significantly alter the precipitation levels as well as airflow direction (Figure 1.2). During positive SAM phases, drier conditions for the Fiordland region may be observed with precipitation levels dropping to 400 mm yr^{-1} less than average in response to the enhanced northeasterlies depositing much of the moisture on the North Island (Figure 1.3). In contrast, during negative SAM phases, the subpolar westerlies are strengthened and produce anomalously high precipitation levels up to 400 mm yr^{-1} greater than average (Figure 1.3). El Niño years induce a moderate enhancement of precipitation (up to 200 mm yr^{-1} greater increase) as a result of a northward displacement of the subpolar westerlies and strengthened southwesterly airflow across New Zealand (Figure 1.4). La Niña years tend to increase precipitation with values up to 400 mm yr^{-1} greater than average as a result of an anomalous northerly airflow depositing most of the collected moisture over the Fiordland region in the Southern Alps (Figure 1.4) (Ummenhofer and England, 2007).

Precipitation and Temperature Trends

The Intergovernmental Panel on Climate Change (IPCC) has recorded that New Zealand's mean air temperature has increased by 1.0°C over the period 1855 to 2004 and by 0.4°C since 1950 in association with 20th century warming seen globally (Figure 1.5) (IPCC, 2007). From 1951 to 1996, the number of cold nights and frosts declined by 10 to 20 days per year, paralleling an increase in Fiordland daily average temperatures of 0.22°C from 1951 to 1990 (Salinger and Griffiths, 2001). Over a much longer time period beginning in 1000 and running through 1900, mean temperature seems to have remained fairly steady and has not thought to have varied more than 0.5°C in either direction (McGlone, 1989). Higher temperatures are often associated with easterly to northeasterly airflow in the Fiordland region while lower temperature correspond to westerly and southwesterly flow (Salinger and Mullan, 1999).

The 20th century has seen two major shifts in atmospheric circulation over New Zealand occuring in 1950 and 1976 (Salinger and Mullan, 1999). From 1930 to 1950 the country experienced relatively stronger southwesterly circulation, followed by increased easterly and northeasterly airflow from 1951 to 1975 causing an initial increase in precipitation in Fiordland followed by a relative reduction. Additionally, the 1951-1975 period experienced an increase in national average temperatures of 0.58°C (Salinger and Mullan, 1999). These two periods are presumably linked to changes in the relative dominance of positive and negative phases of SAM and ENSO, which are known to alter the strength of the westerly wind circulation (Figure 1.5). From 1976 through 1994, westerly and southwesterly airflow became more prevalent due to increased frequency in El Niño associated with global warming-induced temperature increases inducing precipitation 10 percent greater than previously recorded (Salinger and Mullan, 1999; Ummenhofer et al., 2009). When compared with paleoclimate records, there is a discernible increase in the

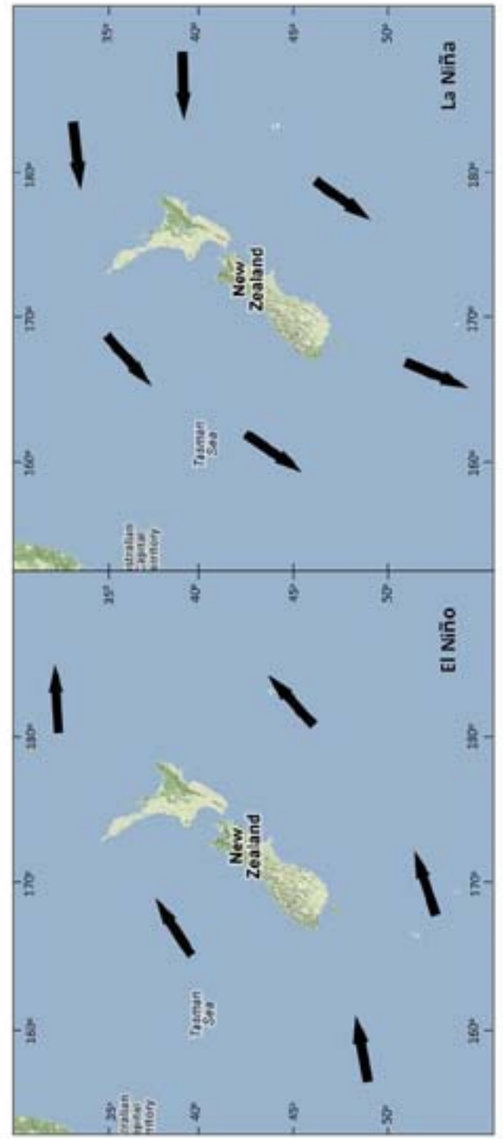

Figure 1.4: Resulting atmospheric circulation patterns and wind flow from the El Niño Southern Oscillation (ENSO). El Niño phase (left) is characterized by enhanced southwesterlies and La Niña phase by anomalously northerly airflow (right), modified from Google Maps (2012).

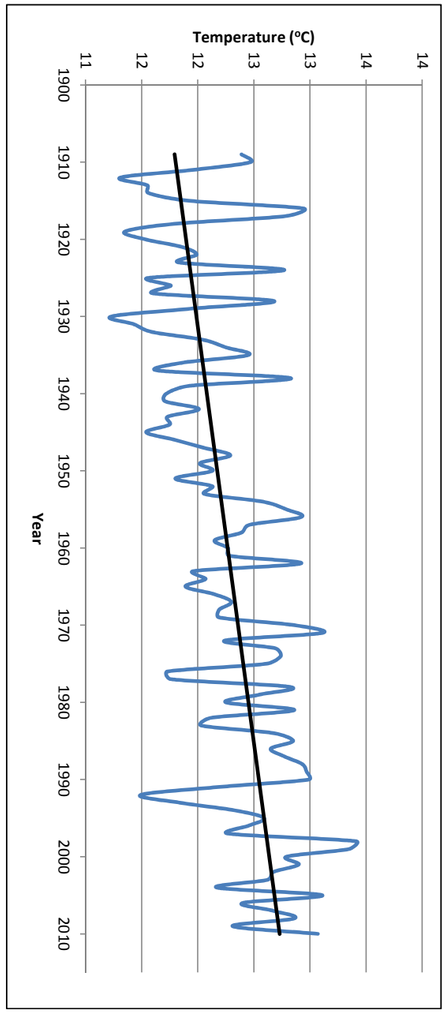

Figure 1.5: New Zealand annual temperature trend from 1909 through 2010 averaged from 7 locations (Auckland, Masterton, Wellington, Hokitika, Nelson, Lincoln, and Dunedin) showing an increase of about 1oC over the past century. Trend is a linear regression model. Data from the National Institute for Water and Atmospheric Research (NIWA), http://www.niwa.co.nz/our-science/climate/information-and-resources/nz-temp-record/seven-station-series-temperature-data.

frequency of El Niño events during recent geologic history (Ummenhofer et al., 2009). Similar to the increasing frequency of El Niño events, recent decades have shown an upward trend in the positive phase of SAM linked to both an increase in greenhouse gas emissions and stratospheric ozone depletion (Ummenhofer et al., 2009). As atmospheric carbon dioxide levels continue to increase, a strengthening of the positive SAM is projected, though the effect of carbon dioxide levels is not currently clear (Cai et al., 2005). In terms of the ozone layer, thinning leads to reduced temperatures over the polar cap, a stronger stratospheric polar vortex and increased SLP gradient between the high and midlatitudes. As previously stated, a positive phase of SAM ultimately results in drier conditions in Fiordland and in light of this recent trend, may be expected to worsen in the future (Ummenhofer et al, 2009).

Climate change is expected to have a profound effect on climate extremes as small changes in mean conditions can amplify the frequency of events like SAM and ENSO (Salinger and Griffiths, 2001). High temperatures can exacerbate drought conditions, increasing the likelihood of forest fires while lower temperatures may result in increased frost and snowfall events. Increased rainfall may also lead to more severe river flooding, inundating more land, bringing changes to terrestrial and aquatic ecosystems (Salinger and Griffiths, 2001).

Fiordland Geology

Two major tectonic structures exist in the Fiordland region of the South Island, the Alpine Fault off the western coast and the Fiordland Boundary Faults, Hauroko and Te Anau, to the east of Pyramid Lake (Hancox and Perrin, 2009) (Figure 1.1). The active Alpine Fault marks the boundary between the sub-ducting Pacific and over-lying Australian Plates and stretches 600 km up the western coast of the South Island migrating on land at the northern extent of Fiordland National Park (“Alpine Fault”) (Figure 1.1). The fault has resulted in the uplift of the Southern Alps, a steep and rugged mountain belt ranging from 1300 to 1500 meters in elevation and occupying the inland region of the Alpine Fault on the South Island (Figure 1.1). It currently moves horizontally at a rate of approximately 3 meters every 100 years (Hancox and Perrin, 2009; “Alpine Fault”). In contrast, the Hauroko and Te Anau faults have had a relative period of quiescence with most recent movements occurring in the Late Cenozoic. The combination of both of these fault zones, though primarily the Alpine Fault, makes the tectonic activity in the Fiordland region of New Zealand particularly active having had three earthquakes greater than magnitude 7 (1939, 1960, 2003) and eight greater than magnitude 6 in the past 150 years (Hancox and Perrin, 2009).

Study Site

Pyramid Lake is located on the outskirts of Fiordland National Park (45°44’S, 167°21’25”E), in southwestern South Island, between the larger Lake Manapouri (Figure 1.1) to the north and Lake Monowai to the south (Figure 1.1 and 1.6) (Mark et al., 2001). It lies about 30 km southwest of the nearest town and tourist center of Manapouri and about 26 km due west of the nearest major road, Blackmount-Redcliff Road (Google

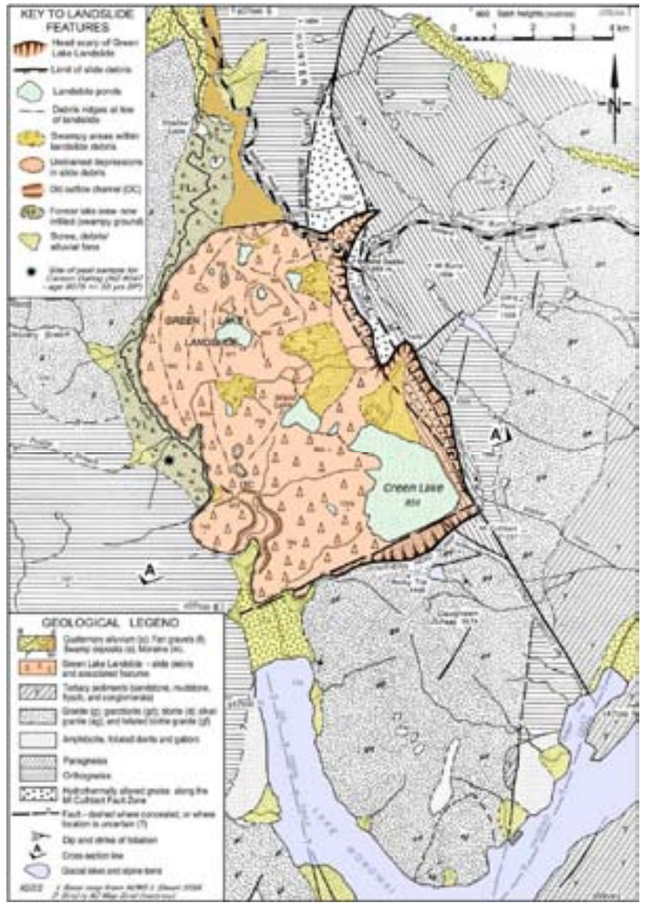

Figure 1.6: Geologic map showing the location of Pyramid Lake (marked by red dot) within the Green Lake Landslide just west of Borland Saddle and south of Borland Road, modified from Hancox and Perrin (2009). A-A' transect denotes position of cross-section in Figure 1.8.

Maps, 2012). Situated at an elevation of 740 meters above sea level, Pyramid Lake is a small, semi-closed glacial lake that has formed in the slide debris of the Green Lake Landslide. There is one inlet on the upper north-east shoreline which periodically drains the tussock peatland field to the east which crosses the scree and alluvial fans of the Green Lake Landslide headscarp (Figure 1.7) (Anderson, 2012; Mark and Dickinson, 2001). With no apparent outlet stream(s), the lake drains through the surrounding landslide debris (Figure 1.7) (Mark and Dickinson, 2001). Additionally, the lake has been shown to be highly susceptible to the effects of evaporation, with water levels changing by as much as 3 meters seasonally (Anderson, 2012). Stretching 500 meters from the southern to northernmost shoreline, the lake contains two sub-basins, the southern and northern with respective depths of 8.5 and 7 meters (Figure 1.8). On the east side of the lake across the low-lying tussock fields rises the Borland Saddle at an elevation of 990 meters above sea level and to the left an unnamed peak at an elevation of 940 meters above sea level ("Green Lake Track"; Google Maps, 2012).

Study Site Geology

Pyramid Lake formed 12,000 to 13,000 years ago following the end of the last ice age, the Otiran glaciation. Today it is situated atop remnants of the Green Lake Landslide, the largest known translational rock landslide and wedge failure of its kind on Earth, covering 45 km^2 with an estimated volume of 27 km^3 (Figure 1.6) (Hancox and Perrin, 2009). 14,000 years ago the local Hunter Mountains extended into this region consisting of Pre-Devonian schistose quartzo-feldspathic paragneiss to the northeast and Devonian and Cretaceous granodiorite to the south. The receding glaciers left Quaternary glacial deposits to the east in Grebe Valley, which were subsequently overlain by swamp deposits (Figure 1.6) (Hancox and Perrin, 2009).

One of the most significant features of the area is the Mt. Cuthbert Fault, striking roughly northwest extending from Lake Monowai to the remaining Hunter Mountains north of the Borland Saddle and dipping 25 – 30^o southwest (Figure 1.9). Today it is associated with a thick, 50 meter zone of weak hydrothermally altered paragneiss. Prior to the landslide, the fault sub-paralleled the foliations in the Hunter Mountains' paragneiss. Additionally, the glacial recession deeply eroded the surrounding geology into over-steepened, unsupported valley walls leaving a glacial lake at the toe of the slope in Grebe Valley to the east. This glacial lake coupled with the characteristically high rainfall of the region elevated groundwater levels, substantially reducing the shear strength along the potential failure plane (Hancox and Perrin, 2009). All together the pre-slide conditions left the southern Hunter Mountains extremely vulnerable to collapse. Seismic modeling sugegsts that the trigger for the complete collapse was most likely due to a large, seismically-induced earthquake in the vicinity of 50 to 100 km, possibly the major Alpine Fault. Ultimately, a 9 km segment of the southern Hunter Mountains released withdebris moving up to 2.5 km laterally and 700 m vertically (Hancox and Perrin, 2009).

Today, this slide debris constitutes the region in which Pyramid Lake is located. It is comprised of variously sized boulders in a finer grained (gravel, sand and silt) matrix, with several large semi-intact blocks of gneiss, schistose gneiss and granodiorite bedrock (Figure 1.6). Due to slide morphology, Hancox and Perrin (2009) identified several zones

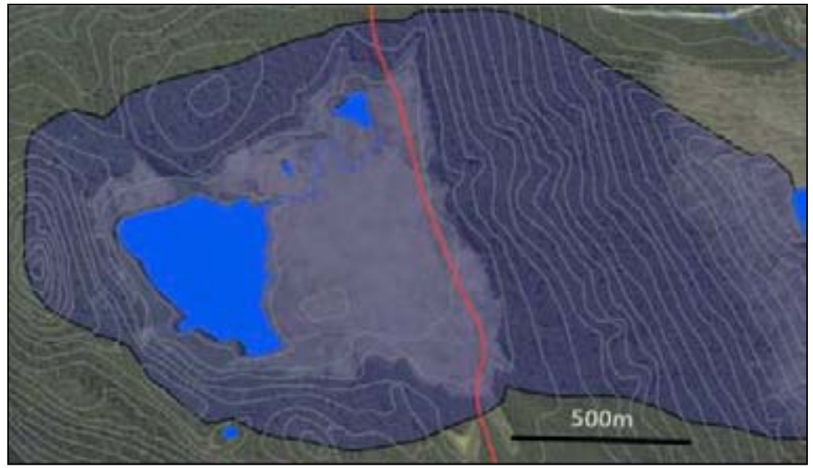

Figure 1.7: Drainage basin for Pyramid Lake where the red line marks the Mt. Cuthbert Fault, from Anderson (2012).

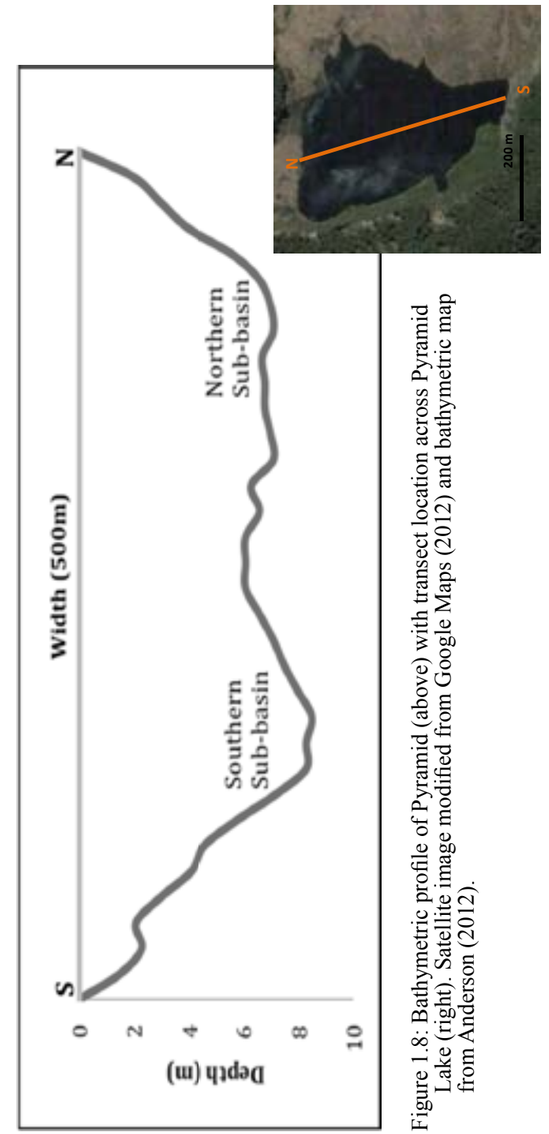

Figure 1.8: Bathymetric profile of Pyramid (above) with transect location across Pyramid Lake (right). Satellite image modified from Google Maps (2012) and bathymetric map from Anderson (2012).

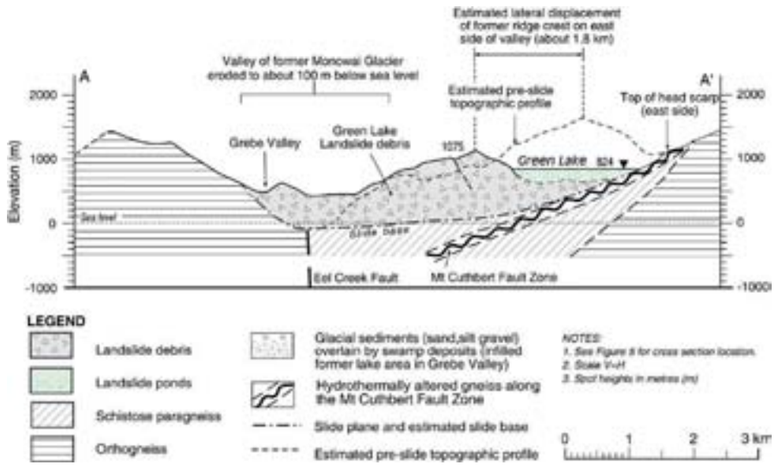

Figure 1.9: Geological cross-section through Green Lake Landslide, from Hancox and Perrin (2009). Note: See Figure 1.6 for cross-section location.

based on debris size . Lake Pyramid is situated atop the head scarp with minimal to no semi-intact blocks or fragmented debris which lie just east of the lake (Hancox and Perrin, 2009).

Vegetation

Based on descriptions of vegetation patterns of the Borland Mire, a 250 ha area of wetland about 14 km due east of the Green Lake Landslide, species of flora could be deduced for the terrain surrounding Pyramid Lake. The main constituents of the flora likely include mountain beech (*Nothofagus solandri* var. *cliffortioides*) forest surrounding the lake and stretching up to higher altitudes on the Borland Saddle and surrounding peaks. The tussock grassland located directly to the east of Pyramid Lake is likely comprised of some variations of blue tussock (*Poa colensoi*), hard tussock (*Festuca novae-zelandiae*) and *Raoulia subsericea* (Mark et al., 1979). A small, periodically-flooded area (c. 200 m^2) adjacent to the inlet stream has been identified and is characterized by the *Deschampsia cespitosa* grass, which is often associated with seasonal flooding and nutrient poor soils (Figure 1.7) (Mark and Dickinson, 2001). Small shrubs of bog pine (*Dacrydium bidwilii*) and manuka (*Leptospermum scoparium*) may be scattered throughout the tussock and increase in abundance approaching the surround mountain beech forests (Mark et al., 1979). Though this is likely the current state of flora, New Zealand's vegetation patterns are strongly influenced by precipitation and air temperatures as the result of variance in the strength and position of the westerlies discussed earlier (Newnham et al., 2012). Additionally, the flora has had a severe impact from anthropogenic forcing in recent history, namely deforestation and the grazing of deer introduced around the turn of the century (McGlone, 1989; Veblen and Stewart, 1982).

Human Settlement

Polynesian (Māori) settlement of New Zealand (c. 1280 AD) is extremely recent when compared to initial human settlement in other regions of the world (McGlone, 1989). Paleoecological records show that both islands were extensively forested prior to the arrival of the Māori; however, by the time the Europeans arrived between 1840 and 1860 forty percent of the lowland and montane forests had been lost (McGlone, 1989). The Māori deforested by setting massive fires which resulted in abrupt changes in vegetation inferred from pollen data and initiated subsequent erosive episodes (McWethy et al., 2009; McGlone, 1989). This period became known as the Initial Burning Period (IBP) which lasted up until about 450 years ago, followed by a relative period of quiescence for about 200 more years. When the Europeans arrived deforestation practices resumed for the purpose of converting forest, fern-shrubland and tussock grasses to pasture for livestock (McGlone, 1989).

Distinguishing between anthropogenic or naturally induced fires is not possible simply by looking at soil charcoal levels, the standard means of fire analysis. In the South Island between 2000 and 6500 years B.P., there were at least six fire outbreaks prior to human occupation of New Zealand, indicating it is not unusual for natural forest fire to occur here. Drier conditions from decreased precipitation and/or elevated temperatures,

as the result in changes of atmospheric circulation, increase the probability of fire episodes (McGlone, 1989). Regardless of origin, forest fires present a significant mode of alteration to surrounding ecosystems by changing vegetation environments effecting other flora and local biota as well as inducing soil erosion (McWethy et al., 2009). In one study, a sharp increase is documented in terrestrial organic matter following the deforestation of the Lake Pleasant, MA watershed around 1780 (Kaushal and Binford, 1999).

The study by McWethy et al. was the first published which documented the fire history in the Fiordland region extending east over to the southeastern hills by means of high-resolution macroscopic charcoal and pollen analysis of sediment cores of five lakes (2001). Results suggest that the high incidents of forest burning occurred in regions in the vicinity of Pyramid Lake only during the Maori settlement period. By the time Europeans arrived fire activity was less pronounced which may be attributed to the fact that there were no forests left to burn or that the Europeans deemed the soil too poor for pasture development (McWethy et al., 2001).

Sediment Records as a Proxy for Climate Change

Nutrients and Biogenic Silica

Phosphorus is an element vital to life on Earth as it is a critical for the creation of any organism, its proper functioning and reproduction. Generally being the least abundant of life's nutritional and structural components (carbon, hydrogen, nitrogen, oxygen and sulfur being the others) it is the most common limiting factor in biological productivity, particularly in freshwater environments (Wetzel, 2001). Phosphorus does not exist in any stable gaseous phase, meaning its residence time in the atmosphere is short since the particulates precipitate out quickly. After being distributed with the soil, phosphorus is generally immobilized by iron, aluminum and calcium, rendering these forms of phosphorus insoluble and inaccessible to plant uptake during photosynthesis (Pierrou, 1976; Wetzel, 2001). Therefore, plant-accessible phosphorus, such as free orthophosphate (PO_4^{3-}), levels are generally low and limiting to plant growth. If levels of phosphorus are high enough, nitrogen may become the limiting factor but only for short periods of time (Pierrou, 1976).

There are various sources of phosphorous deposition into aquatic ecosystems, both natural and anthropogenic. Within the last century, industrial use of phosphorus has become increasingly widespread, ultimately transferring higher than normal levels into aquatic systems up to twice the pre-industrial levels (Filippelli, 2008). Airborne phosphorus delivered to ecosystems by dry-deposition or precipitation generally originates from high-temperature combustion of organic matter, industrial exhaust fumes, human cremation and sea/lake spray. Terrestrial land run-off constitutes the major contributor to aquatic systems transporting organically-bound phosphate in dead and decomposing organic matter as well as incorporating immobilized phosphorus from weathered rocks (Pierrou, 1976; Wetzel, 2001). In addition, sewage containing human and industrial waste products, commonly from the production of dyes, detergents, dairy and canning are becoming increasingly common sources (Pierrou, 1976). A simple

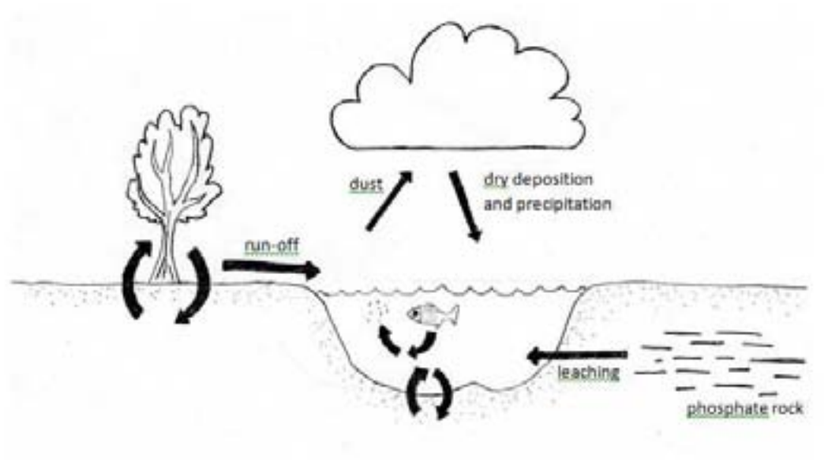

Figure 1.10: Simplified schematic of phosphorus fluxes modified to Pyramid Lake's system. Note: anthropogenic fertilizers are thought to be negligible. Arrows are roughly proportional to rates of transfer.

schematic of phosphorus cycling is illustrated in Figure 1.10 highlighting the sources of phosphorus likely to be contributing to Pyramid Lake's system. Freshwater ecosystems are highly sensitive to additions of phosphorus, since immobilization is significantly more difficult in aquatic settings due to reduced levels of aluminum, calcium and iron (Pierrou, 1976). One sensitivity, primary productivity, is therefore stimulated by influxes of phosphorus and nitrogen; however, nutrient levels must be maintained in order to sustain higher rates of productivity as reduced levels will revert back to pre-nutrient loading conditions within weeks to months (Wetzel, 2001). The rates of productivity may be interpreted by means of biogenic silica (BSi), amorphous silica produced by small siliceous organisms, namely diatoms, which is subsequently incorporated into their frustule (test) and preserved in the sediment (Conley, 1988). Studies have shown nutrient enrichment stimulates diatom productivity and biogenic silica sedimentation while nutrient depletion limits them (Conley, 1988; Conley and Schelske, 2001). If productivity rates increase to the extent at which they deplete the reservoir of dissolved silica then diatom production will be limited by the remaining silica (Schelske et al., 1986). Thus, BSi not only provides an index for diatom abundance, but for lake productivity as well (Conley, 1988).

Organic Matter and Elemental Carbon and Nitrogen

Lacustrine sedimentary organic matter originates from particulate detritus of plants, algae and plankton in and around the lake and constitutes a complex mixture of lipids, carbohydrates, proteins and other biochemical components (Meyers and Teranes, 2001). The accumulated organic matter in sediment records may be interpreted by geochemical analysis of bulk and compound-specific biological components and connected back to established relationships with environmental changes (Fogel and Cifuentes, 1993). Elemental ratios, in terms of C/N, and isotopic ratios, $\delta^{13}C$ and $\delta^{15}N$, elucidate changes in paleoenvironments by illustrating organic matter sources, primary productivity rates and past availability of nitrogen to primary producers (Meyers and Teranes, 2001).

Terrestrial versus aquatic plant sources are one of the main factors which alter and control the C/N elemental ratios in lacustrine organic matter (Figure 1.11). Vascular plants, such as trees, grasses and shrubs found mostly surrounding lakes on land and sometimes in shallow portions of the lake, contain large proportions of fibrous, carbon-rich cellulose and lignin low in nitrogen content. In contrast, non-vascular plants such as aquatic algal phytoplankton contain little to no carbon-rich cellulose but do contain nitrogen-rich proteins and lipids in comparison to their terrestrial counterparts (Meyers and Lallier-Vergès, 1999; Talbot, 2002). Thus, terrestrial versus algal origin can be distinguished based on C/N ratios such that lacustrine algae have a C/N ratio between 4 and 10, whereas terrestrial organic matter has a C/N ratio greater than 20 (Meyers and Teranes, 2001) (Figure 1.11). Therefore, an increase (decrease) in C/N ratios in sediment records generally indicate higher (lower) proportions of terrestrial organic matter compared to aquatic (Meyers and Lallier-Vergès, 1999; Meyers and Teranes, 2001). Additionally, since carbon and nitrogen represent fundamental components to organic matter, concentrations of total organic carbon reflect general abundances of organic matter and total nitrogen concentrations roughly record the total levels of nutrients available (Meyers and Teranes, 2001; Talbot, 2002).

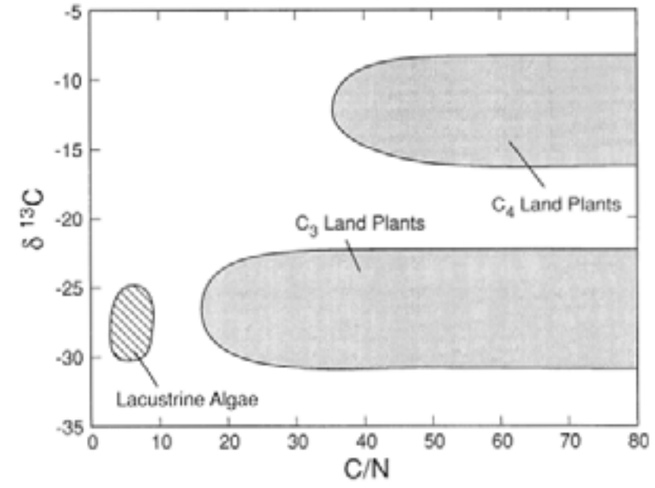

Figure 1.11: Representative elemental and isotopic compositions of organic matter from lacustrine algae, C3 and C4 land plants, from Meyers and Lallier-Vergès (1999).

Carbon Stable Isotopes

Carbon isotopes naturally exist in the form of ^{12}C, ^{13}C, and ^{14}C, which undergoes radioactive decay and thereforewill not be considered here. Isotopic compositions of amaterial are reported in δ values, which are expressed as parts per thousand (per mil, ‰) deviation from a standard, Pee Dee Belemnite (PDB) and atmospheric nitrogen for carbon and nitrogen, respectively (Peterson and Fry, 1987):

$$\delta X = [(R_{sample}/R_{standard}) - 1] \times 1000$$

where X corresponds to the ratio of the heavy to light isotope ($^{13}C/^{12}C$ or $^{15}N/^{14}N$). During photosynthesis, all plants and algae preferentially select for the lighter ^{12}C isotope from the CO_2 in the atmosphere or dissolved CO_2 in the lake, resulting in isotopically depleted ratios with respect to ^{13}C (Peterson and Fry, 1987).

C_3 plants utilize the Calvin-Benson pathway, fixing CO_2 with the ribulose biphosphate carboxylase-oxygenase enzyme (RuBP), resulting in $\delta^{13}C$ values averaging around -27‰ (Sharp, 2007). In contrast, C_4 plants employ the dicarboxylic acid pathway generally producing $\delta^{13}C$ values between -4‰ and -6‰ (Figure 1.11). A third pathway, crassulacean acid metabolism (CAM), is common in desert plants resulting in isotopic discrimination varying between -4‰ and -20‰ (Meyers and Lallier-Vergès, 1999; Sharp, 2007). The C_3 pathway, favored in cooler and dryer climates at higher altitudes, is employed by trees, most shrubs, herbs, cool-weather grasses, phytoplankton and aquatic plants (Sharp, 2007). Based on Pyramid Lake's location, elevation, climate and known vegetation patterns, C_3 plants are likely the sole constituents of terrestrial vegetation contributing to organic matter in the sediments (Mark and Dickinson, 2001; Mark et al., 1979; Salinger and Mullan, 1999).

Lacustrine algae carboxylate dissolved inorganic carbon (DIC) from the surface water, discriminating against HCO_3^- in favor of CO_2, primarily using the RuBP enzyme (Fogel and Cifuentes, 1993). As C_3 plants utilize the same enzyme, typical $\delta^{13}C$ signatures of algae ranging from -25‰ to -30‰ are also observed and therefore source of organic matter cannot be distinguished solely on $\delta^{13}C$ signals (Figure 1.11) (Fogel and Cifuentes, 1993; Meyers and Teranes, 2001). Complications in interpreting recorded $\delta^{13}C$ may arise when the availability of dissolved CO_2 is limited or pH levels are low forcing algal phytoplankton to fix dissolved HCO_3^- ($\delta^{13}C$ = 1‰) (Fogel and Cifuentes, 1993; Meyers and Lallier- Vergès, 1999). This situation is typically seen during periods of high productivity when dissolved CO_2 is severely diminished during increased rates of photosynthesis. In such cases, $\delta^{13}C$ values of algal organic matter may increase up to values of -9‰, which are typically indicative of C_4 plants (Figure 1.11) (Meyers and Lallier-Vergès, 1999).

The $\delta^{13}C$ values of phytoplankton also vary with rates of primary production within lake ecosystems. $\delta^{13}C$ values become enriched with increasing productivity and depleted with lower rates of primary productivity (Brenner et al, 1999; Schelske and Hodell, 1995). In the case of increased productivity as supplies of DIC become depleted during increased uptake, the $\delta^{13}C$ values of the remaining DIC pool increase and produce subsequently higher $\delta^{13}C$ signatures in the newly produced organic matter. With lower rates, primary producers are not limited by DIC supply and can preferentially select the lighter ^{12}C

isotope (Meyers and Teranes, 2001). Rates of primary productivity may increase (decrease) with nutrient inflow, which may result during periods of enhanced (decreased) precipitation and run-off (Jeng and Marshall, 2004; Wetzel, 2001). Additionally, temperature may act as a control on $\delta^{13}C$ values, where colder environments are characterized by more dissolved CO_2 and therefore more depleted values. Fractionation also decreases with temperature resulting in more enriched values in warmer climates (Fogel and Cifuentes, 1993).

Changes in atmospheric $\delta^{13}C$ values must be taken into account when analyzing sediment cores as the rate of fossil fuel burning and deforestation has increased in the past 200 years. The increased projection of fossil fuels relatively enriched in ^{12}C into the atmosphere, known as the Suess Effect, has depleted the atmospheric $\delta^{13}C$ values by about 1.4 per mil since 1840, thus altering the $\delta^{13}C$ signature of dissolved inorganic carbon available to both terrestrial and aquatic plantlife (Figure 1.12) (Schelske and Hodell, 1995). In several recent studies, it was illustrated that the alteration of $\delta^{13}C$ via the Suess Effect in Lake Tanganyika and a selection of Florida lakes must be corrected to obtain accurate interpretations of sediment core $\delta^{13}C$ signatures (Schelske and Hodell, 1995; Verburg, 2007).

Nitrogen Stable Isotopes

Though not as widely used as $\delta^{13}C$ in paleolimnological studies, nitrogen isotopic composition, defined as $\delta^{15}N$ corresponding to ratios of $^{15}N/^{14}N$, can similarly help distinguish terrestrial versus aquatic organic matter sources and past productivity rates by the availability of varying forms of nitrogen to primary producers (Meyers and Teranes, 2001; Peterson and Fry, 1983). During photosynthesis, incorporation of different nitrogen sources (i.e. N_2, NO_3^-, NO_2^-, NH_4^+) results in distinct fractionations, making it possible to track nitrogen sources in lakes (Figure 1.13) (Fogel and Cifuentes, 1993). Atmospheric nitrogen, N_2 ($\delta^{15}N$ = 0‰), is generally removed or fixed from the atmosphere by microorganisms living symbiotically in higher terrestrial plants, and since isotopic fractionation does not occur at this stage, C_3 photosynthesizers generally exhibit a $\delta^{15}N$ signature of 0.5‰ (Meyers and Teranes, 2001). In aquatic settings, non-nitrogen-fixing phytoplankton assimilate dissolved inorganic nitrogen (DIN) commonly in the form of nitrate, NO_3^- ($\delta^{15}N$ = -4‰ to 4‰), although nitrite (NO_2^-) and ammonium (NH_4^+) are also assimilated, producing a signature of around 8.5‰ (Figure 1.14) (Fogel and Cifuentes, 1993; Meyers and Teranes, 2001).

The $\delta^{15}N$ signal of algae, like $\delta^{13}C$, also increases (decreases) with increased (decreased) rates of productivity (Meyers and Teranes, 2001). In the case of increased productivity, as supplies of dissolved inorganic nitrogen (DIN) become depleted during increased uptake in favor of isotopically heavy ^{15}N, the $\delta^{15}N$ values of the remaining DIN pool increase and produce subsequently higher $\delta^{15}N$ signatures in newly produced organic matter. With lower rates of productivity, the phytoplankton have the option to discriminate against the heavy ^{15}N, ultimately resulting in a relatively depleted signature (Talbot, 2002). $\delta^{15}N$ values have been shown to decline upon hypereutrophication resulting from N_2 fixation by cyanobacteria which tend to flourish under these conditions (Brenner et al., 1999). The complicated nature of isotopic nitrogen composition makes

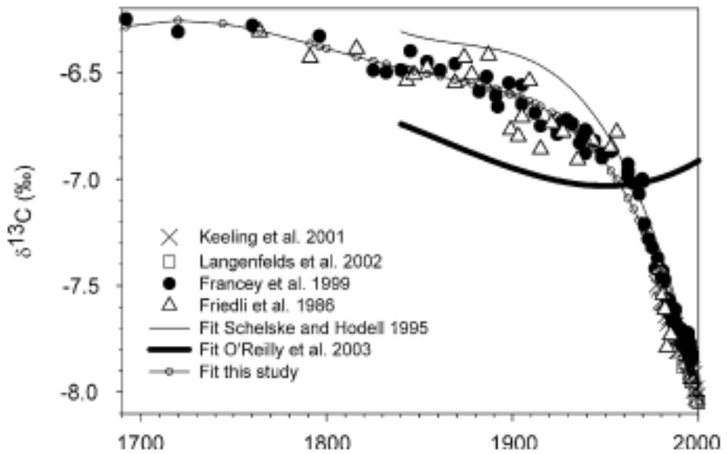

Figure 1.12: Suess Effect shown as the change in atmospheric δ13C by anthropogenic activity with several data sets indicated (n = 160) spanning the last several centuries. Keeling et al. analyzed air samples from 10 sites spanning from the Arctic to the South Pole (2001) while Langenfelds et al. analyzed flask air samples from the Commonwealth Scientific and Industrial Research Organisation's (CSIRO) Global Atmospheric Sampling Laboratory (GASLAB) (2002). Francey et al. (1999) analyzed air collected from Antarctic ice core and firn samples, as did Friedli et al (1986). Several slope fit models are shown, indicating the increasingly isotope depleting effect, from Verburg (2007).

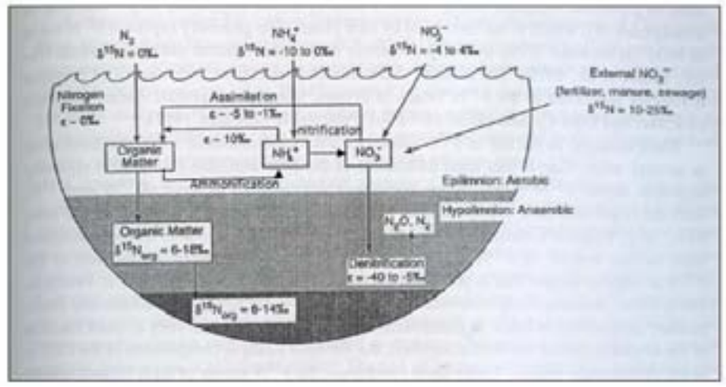

Figure 1.13: Idealized nitrogen isotope cycle schematic of a small, stratified lake. Note that fractionation does not occur during N-fixation of atmospheric N2 by algae. Enrichment factors, ε, are from Fogel and Cifuentes (1993) where negative values represent a depletion of the product relative to the substrate, modified from Meyers and Teranes (2002).

its use as a primary productivity proxy unideal. Therefore, when used in conjunction with other proxies such as carbon isotopes and elemental ratios between the two, sounder conclusions pertaining productivity may be reached.

An important aspect to consider is that anthropogenic influences such as fossil fuel combustion discharge gaseous and particulate nitrogen into the atmosphere, and agricultural and urban development add significant amounts of dissolved nitrogen to terrestrial and aquatic ecosystems in the form of organic and artificial fertilizers (Talbot, 2002). Organic fertilizers have $\delta^{15}N$ values ranging from 6‰ to 30‰ while artificial fertilizers, synthesized from atmospheric N_2 source, show values in the range of -4‰ to 4‰ (Fogel and Cifuentes, 1993). Therefore, nitrogen isotope signatures should represent some degree of anthropogenic influence in the organic matter content of aquatic and terrestrial plants. If fertilization is high (low), productivity rates, total nitrogen and isotope signals should correlate accordingly (Fogel and Cifuentes, 1993).

Compound-Specific Lipids

Lipids constitute molecular membrane components of bacteria, algae, vascular higher plants leaf waxes (HPLW), and persist in sedimentary records over large geological timespans while retaining their source information (Chikaraishi et al., 2004; Sauer et al., 2001). The specific compounds within the lipids termed biomarkers may be used to infer the principal sources of organic matter. Due to the robust nature of most compounds and their high resistance to microbial degradation when compared to other types of organic matter, biomarkers are becoming increasingly popular as proxies for organic matter source (Chikaraishi et al., 2004). Common biomarkers include aliphatic (open-chain) hydrocarbons, carboxylic acids, alkanols, sterols, polycyclic aromatic hydrocarbons (PAHs), pigments and lignin derivatives (Meyers, 2003).

In terms of aliphatic hydrocarbons (*n*-alkanes), odd over even (OOE) chain lengths tend to dominate. Aquatic algae and photosynthetic bacteria are typified by C_{17} chains, where the relative abundance is representative of lacustrine paleoproductivity. Submerged aquatic plants and floating macrophytes are commonly recorded by C_{21}, C_{23}, and C_{25} chain lengths while terrestrial vascular plants contain larger proportions of longer hydrocarbon chains (C_{27}, C_{29} C_{31}) in their epicuticular leaf wax coating (Chikaraishi et al., 2004). Relative abundances of these longer chained *n*-alkanes reflect the amount of terrestrial organic matter transported to the lake basin (Meyers, 2003). Additionally, in watersheds where grasses are the dominant species C_{31} is likely to be recorded as major hydrocarbon, while C_{27} and C_{29} typify the dominance of trees (Meyers, 2003).

Carboxylic acids, or alkanoic acids, are common components of biota as well, however, they have a predominance by even over odd (EOF) chain lengths in contrast to their *n*-alkane counterparts. Longer chain length saturated acids ranging from $C_{24:0}$-$C_{30:0}$ originate from the epicuticular waxy coatings of terrestrial plants while $C_{16:0}$ and $C_{18:0}$ acids are major components of freshwater algae (Meyers, 2003). Carboxylic acids, especially those derived from algae, are also much more susceptible to microbial degradation and therefore more useful as indicators of organic matter recycling in sediments. If recycling of organic matter appears to be minimal, they provide a useful tool for measuring amounts of terrestrial and aquatic organic matter accumulation

(Meyers, 2003). Additionally, polyunsaturated acids, such as $C_{18:1}$, have been shown to increase in concentration with decreasing temperatures as organisms favor them to maintain membrane fluidity in cooler and harsher conditions (Kawamura and Ishiwatari, 1981).

$^{239+240}$Pu-dating

At the time of the earth's origin large amounts of ^{244}Pu and ^{239}Pu were present, however, negligible amounts of primordial ^{244}Pu remain and ^{239}Pu has long since decayed away (Ketterer and Szechenyi, 2008). Therefore any plutonium found on the earth's surface today can be attributed to anthropogenic activity within the last six decades. Approximately 1.4×10^{16} Bq (6000 kg) of ^{239}Pu, along with smaller masses of ^{240}Pu, ^{241}Pu, and ^{242}Pu, have been deposited onto the Earth's surface, mainly as a result of atmospheric weapons tests through the 1950's and 1960's (Ketterer and Szechenyi, 2008). A discernible spike in plutonium concentration, generally measured as Bq/kg of $^{239+240}$Pu, is recognized in soils and sediment cores during 1963/64. This is followed by a dramatic decrease in concentrations coinciding with the 1963 Limited Test Ban Treaty signed by the United States, United Kingdom and former USSR (Ketterer and Szechenyi, 2008). With this knowledge, an age model can be constructed for the Pyramid Lake sediment cores based on the start of increased plutonium concentrations beginning around 1953 and a peak and subsequent drop representing the 1963/64 timeframe.

Past New Zealand Lake Sediment Studies

Lake sediments have shown to be excellent recorders of past climates through the geochemical analyses of stable isotopes in conjunction with a number of other proxy indicators such as C/N elemental ratios and biogenic silica. In recent years, numerous paleoenvironmental studies of lake cores have been employed in New Zealand in an effort to link changes seen in the lake sediment record to regional Holocene climate variability, storm frequency and human settlement (Augustinus et al., 2006; Heyng et al., 2012; Page et al., 2010; Striewski et al., 2009). Sedimentilogical evidence from Lake Tutira on the eastern coast of the north island suggests that ENSO and SAM have been highly variable over the last 7200 years producing sudden decade long periods of enhanced storminess proving to be influential in driving the ecological state of the region (Page et al., 2010). Also on the north island, Lake Pupuke in the capital city of Auckland has undergone some considerable research. Geochemistry, stable isotopes and mineral magnetism have been employed to provide evidence for the colonization by the Māori through disturbances within the catchment area and an ongoing state of natural eutrophication beginning prior to settlement (Striewski et al., 2009). Pollen records, diatom stratigraphy and carbon isotopes from the past 190 years also indicate enhanced eutrophication with the onset of European settlement and changes in landuse (Augustinus et al., 2006). In a separate study at Lake Pupuke, stable isotope analysis of bulk organic matter spanning the period since 7165 years BP revealed sedimentation of mainly autochthonous plants and algae. Conditions showed nitrogen-limitation and methane oxidation, possibly as a result of increased seasonality beginning around 6600 years ago the enhancing summer stratification and intensifying winter overturn (Heyng et al., 2012).

Unfortunately, these studies are limited to northern portions of the North Island, a region shown to respond differently to changes in atmospheric circulation patterns than Fiordland in the southwest corner of the South Island (Salinger and Mullan, 1999). A brief undergraduate study conducted on several sediment cores obtained from Pyramid Lake focused on lithological input and sediment provenance, however, did not attempt to draw links to paleoproductivity or regional climate change (Anderson, 2012). Therefore, the multi-proxy approach employed here hopes to elucidate changes in sediment organic matter and primary productivity in response to Late Holocene climate variability on the eastern boundary of Fiordland surrounding Pyramid Lake.

Purpose and Goals

Within recent history, climate change has been apparent globally as well as regionally within New Zealand with increases in frequency of extreme rainfall, drought and temperature expected to continue (IPCC, 2007). With increasing knowledge of how climate variability influences New Zealand's regional precipitation and temperature patterns driven by ENSO and SAM (Salinger and Griffiths, 2001; Salinger and Mullan, 1999; Ummenhofer and England, 2007; Ummenhofer et al., 2009), links may be drawn to environmental signals in lake sediments, recorded as changes in C/N, $\delta^{13}C$ and $\delta^{15}N$ and percent biogenic silica. Paleolimnological analysis of sediment cores utilizing these proxies in Fiordland rare and currently limited. Therefore, this thesis will contribute new multi-proxy evidence for the effects of Holocene climate variability on the internal processes of Pyramid Lake and its surrounding environment. Detailed results and analysis will shed shed light on how the environment surrounding Pyramid Lake has been influenced and how it may respond given time in the face of modern climate change.

Chapter 2: Methods

Field Methods

All field work was conducted during the weekend of May 12 and 13, 2012 at Pyramid Lake. The lake was reached by following Borland Road, an unsealed, narrow and steep gravel road subject to slips, washouts, snow, ice, high winds and fallen trees, for about 30 km to the Borland Bivvy where the Green Lake Track begins. The 2 km track winds southward through beech forests north of the lake, opening to low-lying tussock fields with Pyramid Lake on the right facing south ("Green Lake Track") (Figure 2.1).

A bathymetric profile was created along a north-south transect using a hand-held sonar sensor to identify the basin(s) within the lake, as these areas are typically representative of maximum sediment accumulation (Wetzel, 2001) (Figure 2.1). Measurements were recorded about every 10 meters from an inflatable rowboat by submersing the sonar sensor just below the water's surface. Two sub-basins were identified denoted by orange triangles in Figure 2.1 at depths of 7.0 and 8.5 meters respectively. Surface sediment cores were obtained from each of the sub-basins using a basic 60 cm (6 cm diameter) weighted, gravity core with a flapper valve mechanism triggered by a metal messenger. This device allows the corer to descend through the water column in an opened position and once inserted into the sediment, the valve is closed providing suction on the sampled sediment when extracted. Cores were pulled up by hand at a constant rate, capped just below the surface water and carefully transported back to the Borland Lodge to prevent any stratigraphic disturbance.

Back at the lodge, both sediment cores were immediately sub-sampled using a "push-pop" apparatus (Figure 2.2). The top 5 cm were sub-sampled every ½ cm and the remainder of the cores were sub-sampled every centimeter into individual plastic sampling bags. Back in Dunedin at the University of Otago, samples were frozen and shipped to Bates College in styrofoam boxes packed with frozen gel packs to prevent any thawing and further alteration of sediment content.

Laboratory Methods

Upon returning to Bates College, all laboratory procedures were carried out in the Department of Geology's Environmental Geochemistry Laboratory (EGL). The frozen samples were freeze-dried for at least 48 hours. Samples were then ground and homogenized using a corundum mortar and pestle.

Biogenic Silica

Biogenic silica analysis required pretreatment of samples in order to remove calcium and magnesium carbonates. A slower and gentler approach was employed using a method adapted from Pilskaln and Paduan (1992) and Weliky et al. (1983). A portion of each dry sample (150 – 500 mg) was decalcified by reacting sediment with 1N phosphoric acid (H_3PO_4) and filtering out the decalcified sample through 0.4 micron, pre-weighed Nuclepore filters. Filters and de-calcified sediment were then dried at 60°C for at least 12 hours and allowed to cool in a desiccator for a minimum of four hours. A rough estimate of inorganic carbon in each sample was obtained by using the following equation:

Figure 2.1: North-south transect used at Pyramid Lake to create the bathymetric profile. The two sub-basins where cores were collected are identified by the orange triangles with respective lake depths, modified from Google Maps (2012).

Figure 2.2: Author sub-sampling a sediment core with a colleague from the University of Otago at the Borland Lodge using the “push-pop” apparatus.

$$\frac{\text{(initial sample mass) – ((decalcified sample and filter mass) – (filter mass))}}{\text{Initial sample mass}} * 100$$

The silica extraction method is adapted from Leinen (1977), Eggimen et al. (1980) and Mortlock and Froelich (1989) while the spectrophotometric technique is adapted from Parsons et al. (1984). For the extraction procedure approximately 5.0 mg of freeze-dried, decalcified sediment sample was digested with 1.0M sodium carbonate (Na_2CO_3) for 3 hours in a heated water shaker bath at about 85^{o}C. The aqueous silica solution was then filtered out using 0.45 micron Tuffryn filters on a plastic filtration apparatus. One drop of methyl orange pH indicator solution was added followed by 6N hydrochloric acid (HCl) turning the filtrate from a yellow to a pink color with a pH of approximately 3.4.

In order to run samples on the spectrophotometer, a 0.1 mL aliquot of the sample extract solution was added to 2.9 mL of E-Pure water. A series of three solutions, Molybdate (0.1 mL), oxalic acid (0.1 mL) and ascorbic acid (0.05 mL), were then added. The Molybdate solution reacts with the dissolved silica to create a silicomolybdate complex, the oxalic acid prevents interference from phosphates and silicomolybdate complex is reduced to a “molybdum blue” with the ascorbic acid (nasl.cbl.umces.edu, 2012). The intensity of blue color is therefore proportional to the amount of silica in the extract. These samples were transferred to cuvettes which were subsequently measured for absorbance on a Beckman DU 800 spectrophotometer with visible light at both 810 and 820 nm wavelengths through a 1 cm path length quartz cell.

A series of standards was run alongside samples in order to quantify the absorbance measurements as parts per million of silica. The silica was finally calculated as a percentage of the decalcified sediment as follows:

$$\frac{\text{(silica concentration)}(10^{-6}) * \text{(dilution factor)(sample volume)} * 100}{\text{Initial sample weight}}$$

where silica concentration of extract is measured in ppm, initial sample weight is in grams measured at the beginning of the extraction procedure, and sample volume is in mL measured at the end of the extraction procedure. The dilution factor of 32.5 was calculated from the final volume of analyzed sample, 3.25 mL, divided by the sample extract volume of 0.1 mL.

Stable Isotopes

All samples were run on a Costic 4010 Elemental Analyzer (EA) interfaced via combustion (c) to a Delta V Advantage Isotope Ratio Mass Spectrometer (EA-C-IRMS). Between 4 and 5 mg of sediment sample were weighed out on a microbalance into small, tin cups and folded into themselves to prevent sediment loss. Each batch of samples included a set of standards; acetanilide, caffeine and freeze-dried cod muscle tissue of well-established isotopic compositions at the beginning, in the middle and at the end of each run. In addition, a blank tin cup was included with the first standard group.

Considering the historic depletion of $\delta^{13}C$ as a result of fossil fuel burning, measured $\delta^{13}C$ values were normalized to account for this activity. The following polynomial equation

models a 1.4 permil depletion in $\delta^{13}C$ since 1840 (Schelske and Hodell, 1995):

$$\delta^{13}C = -4577.8 + 7.3430t - 3.9213 \times 10^{-3}t^2 + 6.9812 \times 10^{-7}t^3$$

where t is time in years AD. After calculating the relative depletion at a given time interval, this value was subtracted from the measured $\delta^{13}C$ value for each dated sediment sample.

Compound-Specfic Lipids

Total Lipid Extraction

Eight ground and homogenized sediments samples of known mass were selected throughout core 12PL5 and transferred to muffled sintered-glass thimbles. About 200 mL of a 2:1 dichloromethane (DCM):methonal (MeOH) solution and several boiling chips were added to round-bottom flasks. Thimbles containing the sediments were placed inside soxhlet extractors with condensers attached above and the round-bottom flasks sitting in heating mantles below in a hood set at 12°C. Total lipids were extracted from the samples for 48 hours.

Total lipid extracts (TLE) were transferred to separatory funnels suspended in rings stands from the round-bottom flasks, rinsing each three times with DCM. 5% NaCl solution was added to separatory funnels to form a two-phase (water-MeOH/DCM) system. Funnels were capped and shaken vigorously for 30 seconds, periodically releasing any pressure out through stockcocks and set aside to allow the phases to fully separate. The organic phase was drained into the corresponding round-bottom flask. This organic phase extraction process was completed two additional times with fresh DCM added each time. Combined organic extracts were transferred back into the separatory funnels, rinsing the round-bottom flasks three times with DCM and adding 5% NaCl to wash. Solutions were shaken and organic phases drained into clean round-bottom. Samples sat overnight with a small amount of extracted Na_2SO_4 to remove any water. TLE were drained again into round-bottom flasks, pipetted to solvent-rinsed sample vials with Teflon-lined caps and blow-down under N_2 gas.

Saponification

Samples were saponified to liberate the fatty acids from waxes, fats, oils and other complex molecules. TLE were quantitatively transferred, rinsed three times with DCM, to solvent-rinsed screw cap culture tubes and blown down under N_2 gas. About 3 mL of 0.5 N potassium hydroxide (KOH) in MeOH, 1 mL distilled water and several Teflon boiling chips were added to the culture tubes. Sample pH values were checked to insure a strongly basic solution (pH=14). Culture tubes were capped tightly and refluxed in a heating block for two hours at approximately 100°C.

Saponified solutions were transferred to large test tubes, rinsing three times with MeOH followed by three times with hexane. About 3 mL of 5% NaCl and 3 mL hexane were added to solutions, shaken vigorously after each addition, forming a two-phase (hexane/water-MeOH-KOH) system. Solutions were centrifuged at 2,500 rotations per minute (RPM) for three minutes to separate layers. The top hexane layers were drawn off and

transferred to new test tubes. Extraction of the water-MeOH-KOH mixture was repeated twice more, combining all respective hexane fractions in test tubes. About 5 mL of 5% NaCl solution was added to combined hexane fractions, shaken vigorously and centrifuged. Top layers of hexane were drawn off with pipets and transferred to a new test tube. Extraction of NaCl solution with hexane was completed twice more combining TLE neutral fractions with a small amount of Na_2SO_4 to remove any water.

Working with the saved aqueous phase drawn off post centrifuging, the pH was adjusted to about 2 with 10 drops 6 N HCl. The now acidic aqueous phase was extracted three times with about 3 mL hexane, pipetting organic fractions into a new test tube. The combined organic phases (TLE acids) were washed in 5% NaCl solution as done for the TLE neutral previously.

TLE neutrals and acids were transferred to pear-shaped flasks, rinsing the Na_2SO_4 in test tubes three times with hexane and Rotavapping the solvent from the pear-shaped flasks. Samples were transferred to screw-cap vials and evaporated under a gentle stream of N_2 gas.

Esterification of Fatty Acid Methyl Esters (FAME)

Dried TLE acids were esterified by adding 3.6 mL MeOH and 1 mL 14% BF_3/CH_3OH to dried vials, transferring samples to small screw-cap vials and evaporated under N_2 gas. About 1.2 mL of 3% BF_3/CH_3OH was added to vials which were purged with nitrogen gas to expel all air and sealed with Teflon-lined caps. TLE acid reaction mixtures were heated at 100°C for two hours and transferred to screw-cap culture tubes and rinsed three times with MeOH followed by three rinses with hexane. Samples were washed with about 5 mL NaCl solution and three times hexane rinse using the centrifuge as done previously. Top hexane layers were drawn off into pear-shaped flasks and dried overnight with Na_2SO_4. Hexane solutions were Rotavapped to near dryness and transferred to screw-cap vials, rinsing the Na_2SO_4 three times with hexane. Extracts were gently blown-down under N_2 gas.

500 µL of hexane was quantitatively added to each sample and transferred to small auto-vials. For quantification, samples were run on an Agilent 6890-Network flame ionization detector (GC-FID) with two hexane blanks. Concentrations in were calculated using a standard curve as follows:

$$y = 116.25x + 0.8866$$

where y is equal to the area (pA) under the corresponding retention curve and x is equal to the concentration in ng/µL. In order to identify specific compounds, samples were diluted in about 200 µL of hexane and run on an Agilent 6890-Network linked to an Agilent 5937-Network mass spectrometer (GC-MS) with four hexane blanks.

$^{239+240}$Pu Age Dating

Between 0.69 and 1.06 grams from each of the top 15-cm sediment samples from core 12PL1 were collected and shipped to Northern Arizona University for plutonium age dating conducted by Dr. Michael Ketterer. Samples were run on a high resolution inductively-coupled plasma mass spectrometer to measure plutonium concentration (ICP-MS).

Chapter 3: Results

Biogenic Silica

Maintaining consistency in biogenic silica proved to be significantly more difficult than originally expected. Figure 3.1 displays substantial variation of results obtained from three samples, BCID samples 10027, 10065 and 10100, over varying dates between July 27 and November 7, 2012. Initially, biogenic silica was extracted from all decalcified sediments samples and run through the spectrophotometer beginning on 7/27 and finishing on 9/19. As a cross-check, two prepared BSi extracts for 10027, 10065 and 10100 samples were run from stored extracts through the spectrophotometer on 9/25. Relative values for each sample were averaged; however, drastically different results were produced from the first runs (7/27 and 9/19) ranging from 38% to 43% BSi. Considering the large degree of variation the same samples were run again prepared from saved sample extracts on 10/4 producing averaged sample percentages ranging from 38 to 44 which showed remarkable consistency with the results obtained on 9/25. The sharp change in BSi percentages seen between the initial batches and samples run on 9/25 and 10/4 may have been the result of silica leaching while the sample extracts were stored in plastic containers though silica is not known to be an ingredient in the plastic bottle material. To test this theory, both stored sample extracts for each BCID previously run on 10/4 were rerun for a third time on 10/19 in addition to three freshly prepared extracts from the respective decalcified sediment samples. All values between stored and fresh extracts were similar, ranging in average percentages from 7% to 19%, showing consistency with samples originally run on 7/27 and 9/19. This signifies that the hypothesized leached plastic container theory may not have been the culprit for associated error as stored samples would have needed to produce data in the range of those from the previous runs on 9/25 and 10/4. In an effort to further elucidate this source of error, 11 samples including 10027, 10065 and 10100 were rerun from the original stored sample extracts from 7/27 and 9/19 on 11/7 and produced percent BSi percentages ranging from 13% to 49%. Figure 3.1 only displays percent BSi for samples 10027, 10065 and 10100 for 11/7 which seem to be similar to results produced on 9/25 and 10/4.

The complications that arose through this procedure illustrate the high degree of error associated with the laboratory methods and equipment used for determining percent biogenic silica. To make use of the data it was decided to rely upon the results originally obtained on 7/27 and 9/19 (Figure 3.1). Though percent biogenic silica values may not be entirely accurate, the fact that samples were run in only two batches should mean that they display relative levels of BSi with each other. Core 12PL5 shows respectively lower percent biogenic silica values in a near constant, steady trend from about 27 to 14 cm in the middle region of the core (Figure 3.2). Above and below this portion of the core, values oscillate substantially between higher and lower percentages. There appears to be an overall negative trend from the bottom to the lowest observed percentages at about 27 cm and a general positive trend from about 15 cm upwards. Like core 12PL5, core 12PL1 shows a decrease in relative percent biogenic silica from the bottom of the core to about 21 cm (Figure 3.3). At this point values trend towards a more constant state and do not appear to increase near the surface like in core 12PL5. Additionally, 12PL1 does not display the lack of variation seen in the lower percentages of core 12PL5, and instead, oscillates throughout the entire core.

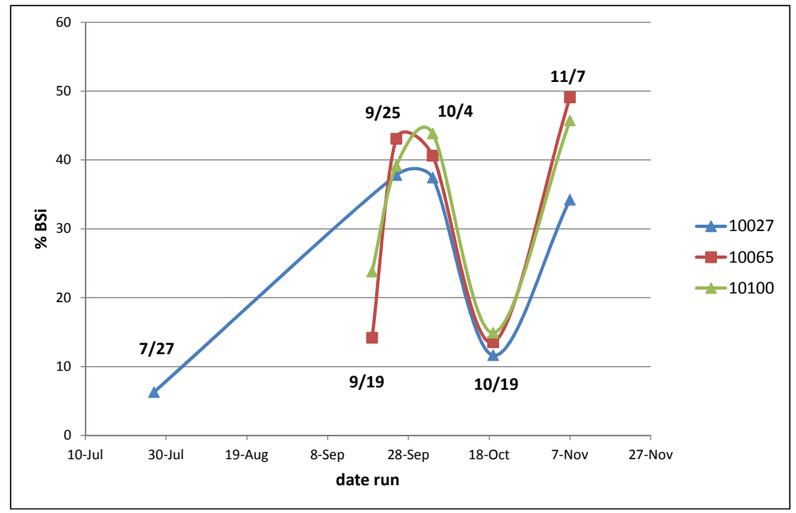

Figure 3.1: Biogenic silica time series for BCID samples 10027, 10065 and 10100.

Figure 3.2: Percent biogenic silica, percent calcium carbonate, percent carbon, δ13C , percent nitrogen, δ15N and C/N elemental ratios for northern sub-basin core, 12PL5, with respect to depth (cm).

Figure 3.3: Percent biogenic silica, percent calcium carbonate, percent carbon, δ13C , percent nitrogen, δ15N and C/N elemental ratios for southern sub-basin core, 12PL1, with respect to depth (cm).

Percent Calcium Carbonate

Core 12PL5 illustrates an overall rise and then fall in percent calcium carbonate up core. From the base of the core up through 15 cm, values fluctuate in a rather positive manner from 12 to 26 % (Figure 3.2). At 15 cm, the trend changes to one characterized by a negative progression up to the surface of the core with the value recorded as 19 %. Core 12PL1 displays an opposite trend such that from the bottom of the core up through 8 cm, a negative trend may be observed from 23 down to 13 % (Figure 3.3). From 8 cm through the surface of core 12PL1 a steady positive trend is shown with values maximizing out at 27 %.

It should be noted that samples 10030, 10032, 10036, and 10038 from core 12PL5 and sample 10082 from core 12PL1 were omitted due to the fact that they either showed negative percentages or exceedingly low values after the decalcified mass was subtracted from the original mass. Negative values are intuitively impossible and the low percentages appeared as extreme outliers which did not fit the observed trends. Biogenic silica samples corresponding to these $CaCO_3$ samples were also omitted as the decalcified masses were used in the biogenic silica calculations and would have thrown off results.

The inverse relationship between percent carbon and $CaCO_3$ seen in core 12PL5 (Figure 3.2) is something to be expected due to natural processes of decomposition of organic matter, acidification of lake waters and subsequent dissolution of calcium carbonates, however, this relationship is not represented in core 12PL1 (Figure 3.3) (Dean, 1999). Therefore, this questions the credibility of core 12PL1's biogenic silica results. The samples may not have been thoroughly dried in the oven during the decalcification procedures or it simply may imply that the two basins are subject to different diagenetic processes. Regardless, the corresponding biogenic silica trends for core 12PL1 displayed in Figure 3.3 must be analyzed with caution and only in conjunction with additional supporting proxies.

Percent Carbon and Nitrogen

Percent carbon and nitrogen values throughout core 12PL5 are displayed in Figure 3.2. Percent carbon values range between 6.7 %, at 15 cm down core, to 13.8 % near the surface. Values below 15 cm appear to oscillate in a fairly constant nature, with a possible slight negative trend. However, above 15 cm, percentages trend positively to the surface. Almost identical trends are seen in the adjacent percent nitrogen graph, though values range from 0.5 to 1.2 % instead, with the lowest value being recorded at 27 cm down core. A positive trend is seen from 15 cm upwards and a slightly decreasing trend from the bottom up to 15 cm down core.

Percent carbon and nitrogen values throughout core 12PL1 are displayed in Figure 3.3. For both sets of data, there appears to be a slight negative trend at the bottom of the core to about 21 cm, followed by a generally steady and positive trend up core with several larger oscillations between 15 and 20 cm down core. Carbon values range from 7.1 to 13.9 % percent and nitrogen values range from 0.5 to 1.1 % percent.

Bulk Stable Isotopes and Elemental Ratios

Stable isotope values of carbon and nitrogen in addition to elemental ratios between carbon and nitrogen are display in Figure 3.2 for the northern sub-basin core, 12PL5. Uncorrected $\delta^{13}C$ values become increasingly depleted towards the surface and range from -27.7 ‰ near the bottom to -29.0 ‰ at the surface of the core. $\delta^{15}N$ values show a slight enrichment moving from the bottom of the core upwards and range from 0.9 ‰ to 1.6 ‰. C/N ratios show on average a more or less invariable trend throughout the core with the lowest ratios recorded at 13.3 and highest at 18.7. Though all graphs seem to show steady trends, there is some oscillations within those trends which should be taken note of.

Figure 3.3 displays similar trends seen in core 12PL5 for stable isotope values of carbon and nitrogen and C/N ratios for the southern sub-basin core, 12PL1. Uncorrected $\delta^{13}C$ values also show a general depletion from the bottom of the core upwards and range from the most enriched value of -27.8 ‰ near the bottom of the core to the most depleted value of-28.7 ‰ near the surface. $\delta^{15}N$ values show a general enrichment upcore and values range from the most depleted of 0.8 ‰ near the bottom to the most enriched of 1.9 ‰ at the surface of the core. Figures for $\delta^{13}C$ and $\delta^{15}N$ also show oscillating values within the respective trends. The C/N elemental ratios for core 12PL1 show a relatively stable and constant trend moving up core with significantly less oscillation than the staple isotopes from both cores and the C/N ratios from core 12PL5. Ratios of C/N for core 12PL1 range from 13.8 to 19.1.

Compound-Specific Lipids

A number of *n*-alkanes were identified in core 12PL5 ranging in carbon chain lengths from 23 to 29, however, no compounds were identified in sample 10046 as a result of sample content lost when the glass test tube shattered during the saponification procedure (Figure 3.4). C_{25} showed by far the greatest relative percentage at any given point ranging from 29 to 47 %. C_{27} and C_{29} represent a moderate proportion of the *n*-alkane composition with relative percentages ranging from 13 to 31 % and from 14 to 29 %, respectively. C_{23}, C_{24} and C_{26} display comparatively low relative percentages ranging from 4 to 12 %, 2 to 6 % and 2 to 11 % respectively. C_{23}, C_{24}, and C_{26} all show similar trends with relatively constant and invariable trends up until about 23 cm while C_{29} decreases. At this depth, all four show a slight increase, plateau out and then decrease in relative percentage at 5 cm from the surface. Conversely, C_{25} increases and C_{27} remains unchanging in relative percentage up to 23 cm at which point they both drop and plateau through 5 cm from the surface. A sharp increase in C_{27} is displayed while C_{25} remains relatively unchanged (Figure 3.4).

The right side of Figure 3.4 displays relative percentages for the identified carboxylic acids in core 12PL5, where dotted lines indicate the unsaturated counterparts of the acids. $C_{16:0}$ shows by far the greatest relative percentage ranging from 19 to 60 % at the surface of the core. Additionally it displays a rather unique trend decreasing up core until 5 cm from the surface upon which the trend increases dramatically. $C_{26:0}$ represents the lowest relative percentage of carboxylic acids up until 19 cm when it increases

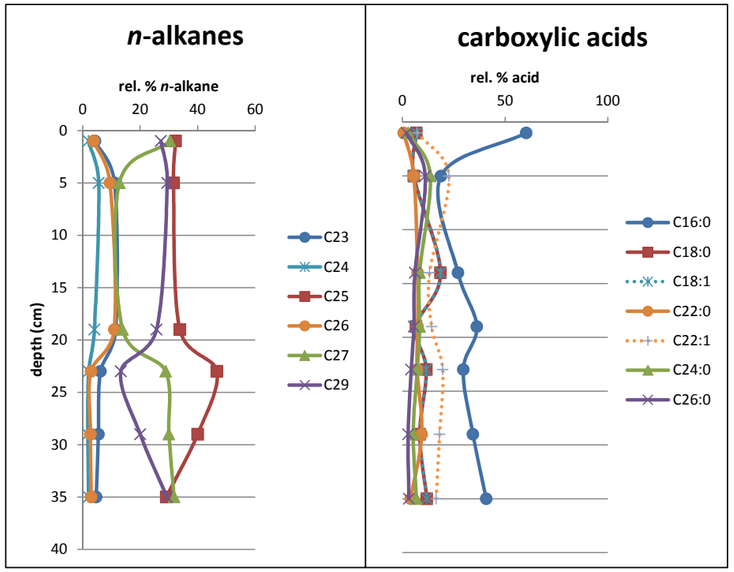

Figure 3.4: Relative percentages of n-alkanes (left) and carboxylic acids (right) from the northern sub-basin core 12PL5 plotted against depth (cm). Dotted lines indicate unsaturated fatty acids.

slightly. At this point $C_{22:0}$ decreases in relative percent and remains the lowest of acids to the surface. With the exception of $C_{16:0}$, the remainder of carboxylic acids shown relatively unchanging trends through 5 cm from the surface at which pint their values drop. Relative percentages for $C_{18:0}$, $C_{18:1}$, $C_{22:0}$, $C_{22:1}$, $C_{24:0}$, $C_{26:0}$ range from 10 to 18 %, 6 to 19 %, 1 to 9 %, 7 to 23 %, 3 to 14 %, and 2 to 11 %, respectively (Figure 3.4).

$^{239+240}$Pu Age Estimates

Concentrations of $^{239+240}$Pu, expressed in bq/kg, for the top 10 cm (n=15) of core 12PL1 are displayed in Figure 3.5. Concentrations remain fairly low and constant at or below 0.1 bq/kg from 10 to 2.5 cm. At 2.5 cm down core, plutonium concentrations begin to rise, peaking at the surface of core with a concentration measured at 2.34 bq/kg.

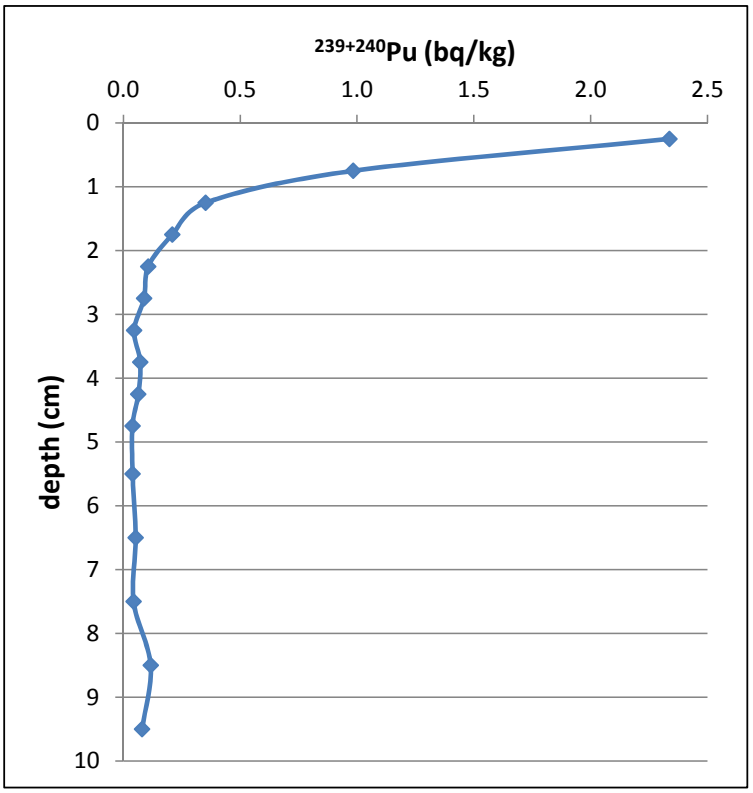

Figure 3.5: $^{239+240}$Pu concentrations (bq/kg) measured for the top 10 cm and 15 samples for the southern sub-basin core 12PL1. Reported by Michael Ketterer, Northern Arizona University (NAU).

Chapter 4: Discussion

Age Model

Pronounced atmospheric deposition of plutonium coincided with increased nuclear weapons testing beginning in the 1950s, such that a rise in $^{239+240}$Pu concentrations found in sediment cores correlates with this time (Ketterer and Szechenyi, 2008). For this reason, sediments at 2.5 cm downcore in core 12PL1, where concentrations display an initial rise after relatively invariable stability, were assigned an age of 1953. Recent sediments should additionally show a spike and subsequent drop in plutonium concentrations coinciding with the 1963 Limited Test Ban Treaty (Ketterer and Szechenyi, 2008). However, such a spike and subsequent drop is not seen in core 12PL1 indicating that the surface of the core deposited after the 1963 timeframe must have been lost. Upon collection of the cores in Pyramid Lake, a water sediment interface was observed and the loss of the uppermost portion of core 12PL1 may be attributed to coring technique which could have pushed away loose or suspended surface sediment as the corer impacted the lake bottom.

In order to produce an age model, the top of core 12PL1 was assumed to represent 1963, resulting in a sedimentation rate of 0.25 cm yr^{-1} for 0 to 2.5 cm. In comparison, Lake Pupuke and Lake Tutira of the north island have sedimentation rates ranging from 0.06 to 0.20 cm yr^{-1} and from 0.31 to 1.53 cm yr^{-1}, respectively (Heyng et al., 2012; Page et al., 2010). Pyramid Lake's sedimentation rate appears slightly greater than Lake Pupuke and slightly less than Lake Tutira which may be attributed to assumptions made in constructing this age model, regional geomorphical features or simply the distinct locations in terms of regional climate effects impacting sediment delivery. Like Pyramid Lake, Lake Tutira formed as the result of a landslide with sediment supply being strongly seasonal and responding rapidly to rainfall-induced erosion in the watershed (Page et al., 2010). With these similarities in mind, the calculated sedimentation for Pyramid Lake appears reasonable. Assuming constant sedimentation through time, ages were extrapolated down core using the sedimentation rate of 0.25 cm yr^{-1}, producing a linear age model for core 12PL1 (Figure 4.1). The plutonium concentration curve in Figure 3.5, which represents the top 15 cm of core 12PL1, illustrates a rapid increase beginning at 2.5 cm and continuing to the surface which is typical of plutonium deposition seen in sediment cores (Ketterer and Szechenyi, 2008). Since there are no unusual features signifying sediment disturbance beyond loss of the most recent 50 years, the surface sediments should therefore be reliable and representative of relative lake conditions.

The top of core 12PL5 cannot be assumed to represent 1963 as it represents a different basin which may be subject to different sedimentation conditions. By comparing proxy data from both cores a sense of correlation or lack thereof can be established. Elemental carbon and nitrogen ratios as well as percent carbon and nitrogen trends from both cores showed similarities in relative fluctuations, however, not at quite the same depths. By assigning the top of core 12PL5 an age of 1961, the bottom an age of 1856 and redistributing the samples in between accordingly both cores appear to correlate significantly better (Figure 4.2). Though the proxies now tend to correlate, amplitudes are not necessarily the same between cores such as the trends in percent carbon and nitrogen seen between 1913 and 1943 and again during the 1950's (Figure 4.2). Lack of precise correlation may be attributed to slight differences in sediment delivery and

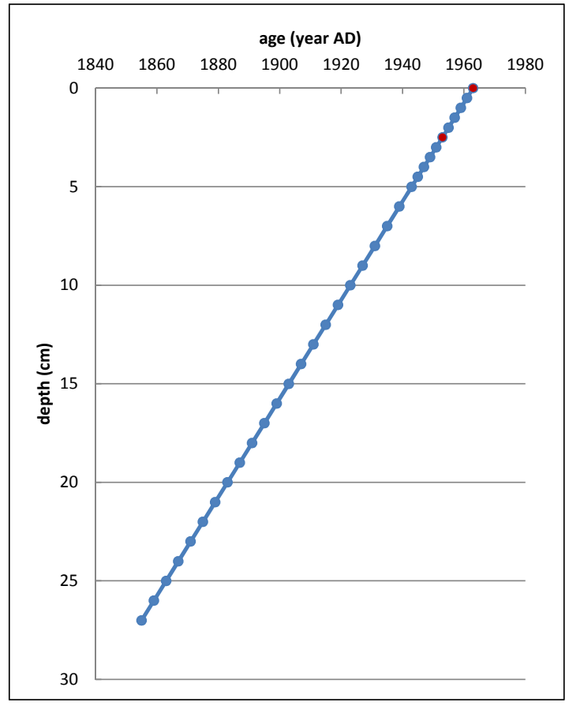

Figure 4.1: Age model for core 12PL1 extrapolated from the surface of the core (age = 1963 years AD) and 2.5 cm down core (age = 1953 years AD).

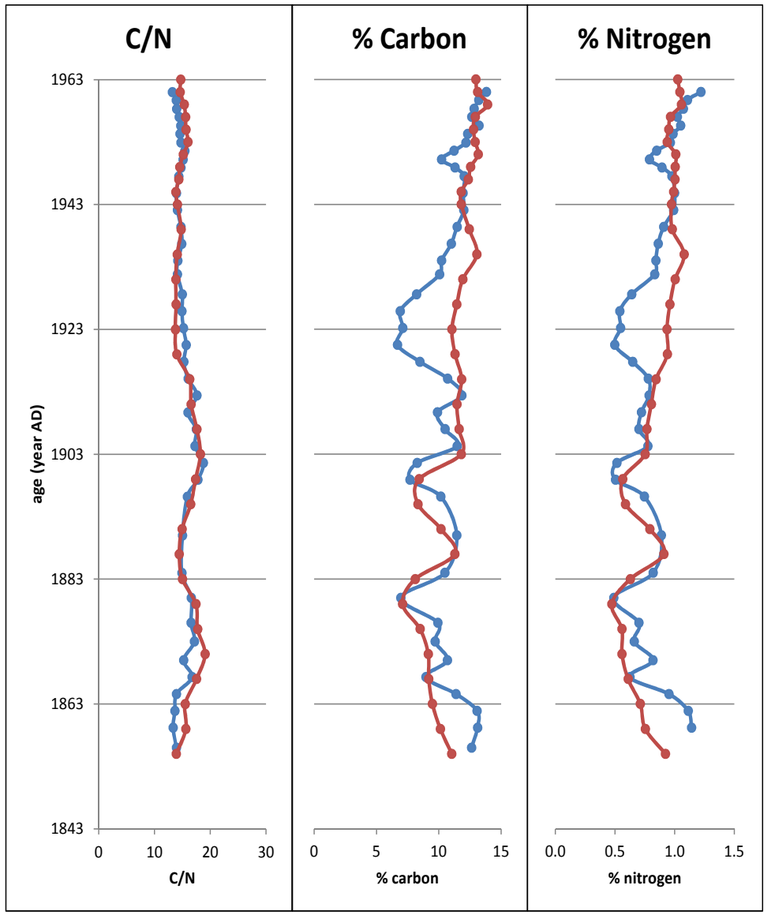

Figure 4.2: Comparison of elemental carbon/nitrogen ratios (left), percent carbon (middle) and percent nitrogen (right) from core 12PL1 (red) and core 12PL5 (blue) after correlating the ages of 12PL5 to 12PL1.

deposition and/or diagenetic processes between the two core locations. Additionally, core 12PL5 is a longer core, however, after proxy correlation the sediments represent roughly the same timeframe, 1855 to 1963 for 12PL1 and 1856 to 1962 for 12PL5 (Figure 4.2). This may indicate more sediment delivery to the northern sub-basin (12PL5) compared to the deeper southern sub-basin (12PL1) or, alternatively, more compaction of core 12PL1 during core acquisition. Regardless, C/N ratios and percent carbon and nitrogen trends for both cores mimic each other in the general sense, suggesting that recent paleoenvironmental conditions expressed in these two cores are accurately represented (Figure 4.2).

Organic Matter Provenance

Sedimentary records are strongly influenced by physical features of the landscape such as lake morphology and watershed topography as well as the relative abundances of lacustrine and terrestrial plant-life and the degradation of that starting material within the watershed (Meyers and Lallier-Verges, 1999; Meyers and Teranes, 2001; Wetzel, 2001). Regional climate, particularly precipitation, serves as a means of transport for organic matter and nutrients from the surrounding drainage basin especially during heightened storm periods when streams and river channels are inundated returning increased levels of organic matter and nutrients to the lake system (Wetzel, 2001). Geologic features and topography of landscape govern the direction of ground and surface water towards the lake basin which represents the lowest point within the watershed (Wetzel, 2001). Considering the lack of outlets observed in Pyramid Lake, the multiple basins identified (Figure 1.8) are good organic matter traps for allochthonous organic matter from the mountain beech forests located on the higher elevations surrounding the lake and the adjacent tussock field to the east (Figure 1.7) (Mark and Dickinson, 2001; Mark et al., 1979). The fluvial runoff originating from the high levels of recorded precipitation, in excess of 6,000 mm yr-1 (Hancox and Perrin, 2009), in the Fiordland region of New Zealand would therefore serve as an adequate vehicle for transportation of large amounts of allocthonous organic matter into Pyramid Lake.

With this in mind, organic matter sources may be interpreted by ratios of C/N, such that that lacustrine algae are typically signified by C/N ratios between 4 and 10, whereas terrestrial organic matter typically show C/N ratios greater than 20 (Meyers and Teranes, 2001). When plotted against corrected $\delta^{13}C$ a proportion of C_3 and C_4 carboxylating vascular plant sources may be illustrated. In Figure 4.3, the C/N ratios and carbon isotopic signatures reveal that Pyramid Lake's organic matter originates from a mix of terrestrial/aquatic C_3 plants and lacustrine algae with proportions leaning more towards the vascular plants. A predominance for terrestrial and/or vascular plant derived organic matter is further supported by $\delta^{15}N$ signatures closer to zero as C3 land plants generally show $\delta^{15}N$ values of 0.5 ‰ while algae are typified by values closer to 8.5 ‰ (Figures 4.4 and 4.5) (Meyers and Lallier-Verges, 1999; Peterson and Howarth, 1987). The significant presence of C_3 plants makes sense considering the temperate climate of Fiordland which would favor trees, most shrubs, herbs, cool-weather grasses, phytoplankton and aquatic plants which all employ the Carbon-Benson pathway (Sharp, 2007). Additionally the three figures, C/N versus $\delta^{13}C$ and $\delta^{15}N$ and $\delta^{13}C$ versus $\delta^{15}N$,

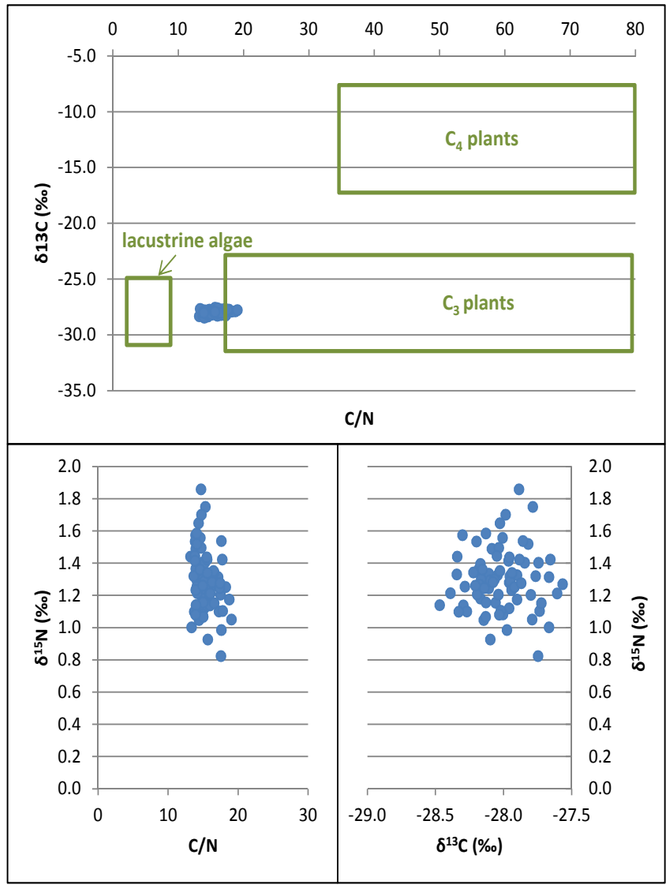

Figure 4.3: Representation of organic matter sources based on the isotopic signature of carbon and elemental C/N ratios (top, modified from Meyers and Lallier-Vergès (1999)) and nitrogen stable isotopes versus C/N ratios (bottom left) and carbon and nitrogen isotopes (bottom right) for cores 12PL1 and 12PL5.

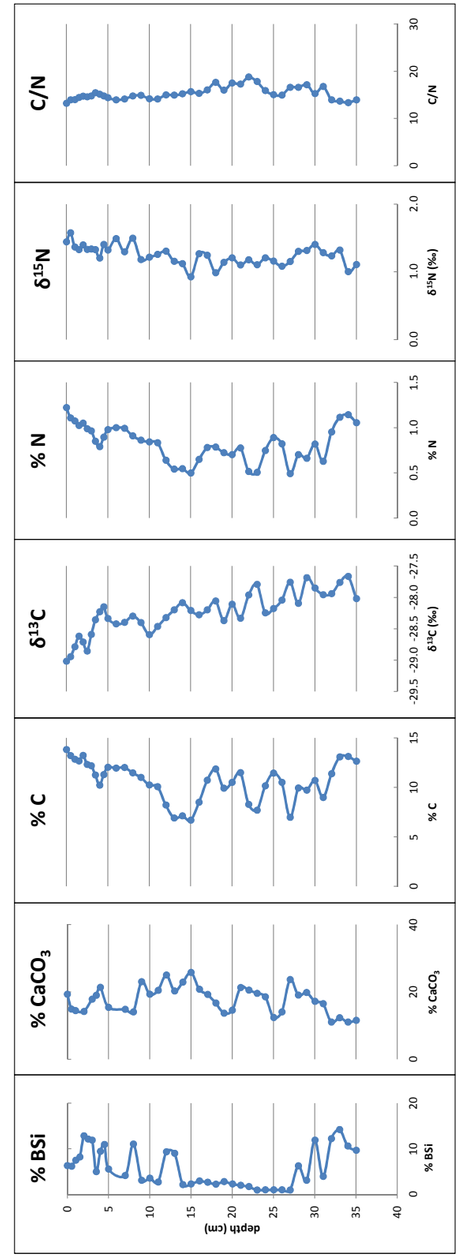

Figure 4.4: Percent biogenic silica, percent calcium carbonate, percent carbon, percent nitrogen, $\delta^{15}N$ and C/N elemental ratios for northern sub-basin core, 12PL5, with respect to age (years AD). Effect), $\delta^{13}C$ (dotted = measured, solid = corrected for Suess

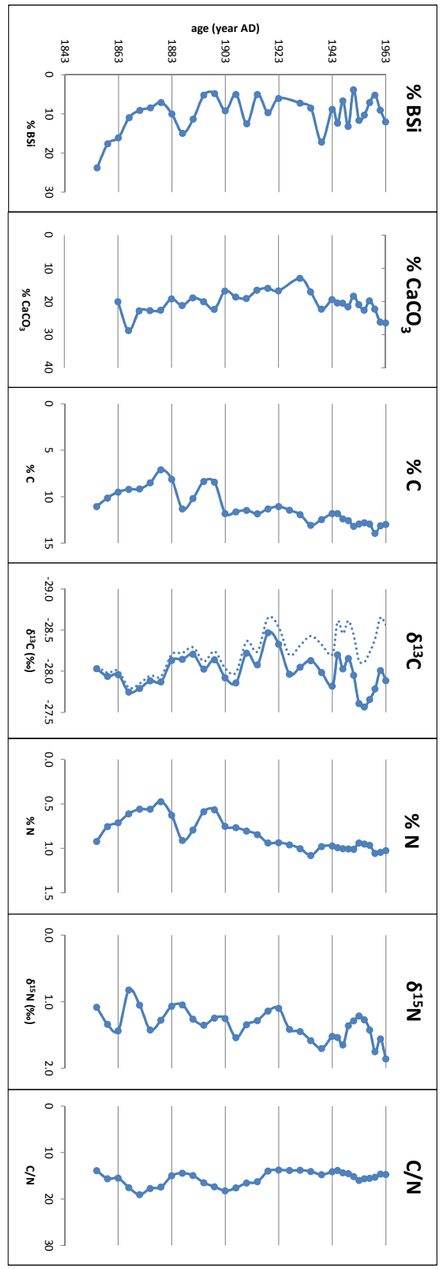

Figure 4.5: Percent biogenic silica, percent calcium carbonate, percent carbon, $\delta^{13}C$ (dotted = measured, solid = corrected for Suess Effect), percent nitrogen, $\delta^{15}N$ and C/N elemental ratios for southern sub-basin core, 12PL1, with respect to age (years AD).

illustrate that all deposited organic matter is of the same origin during this time frame as values are clustered together with no additional groupings suggesting other secondary origins (Figure 4.3).

Trends seen in the C/N ratios up core and through time in Figures 4.4 and 4.5 for cores 12PL5 and 12PL1, respectively, demonstrate a fairly consistent and unchanging source of organic matter. Core 12PL5 exhibits a small drop in C/N ratios from about 1880 to 1900 followed by a slight decrease up core possibly suggesting a period of increased algal organic matter (Figure 4.4). Core 12PL1 also shows a drop in C/N ratios at about the same time from about 1870 to 1903, but seems to more or less stabilize through 1963 (Figure 4.5). Interestingly these periods in both cores are matched by increases in percent carbon and nitrogen, which can generally be interpreted as increases in organic matter and possibly periods of increased primary productivity (Meyers, 2003; Meyers and Teranes, 2001) (Figures 4.4 and 4.5).

An additional proxy for sedimentary organic matter may be expressed through compound-specific lipid analysis of n-alkanes and carboxylic acids. Figure 4.6 illustrates the relative percentages of these compounds versus age down core for the northern sub-basin core 12PL5. N-alkanes identified in Pyramid Lake constitute large proportions of epicuticular waxy coatings originating from submerged aquatic vascular plants ($C_{23,25}$) and terrestrial plants ($C_{27,29}$) and show a relatively equal mixture of the two (Figure 4.6) (Chikaraishi et al., 2004; Meyers, 2003). The presence of longer chain, tree-derived n-alkanes and lack of grass-derived n-alkanes (C_{31}) is similar to the local flora of predominantly mountain beech forests (Mark and Dickinson, 2001; Mark et al., 1979). Additionally, algal and bacterial derived n-alkanes (C_{17} and $C_{12\text{-}22}$, respectively) were not identified supporting the higher C/N ratios (Figures 4.3) typical of vascular plant dominated organic matter (Meyers, 2003).

In contrast to the n-alkane record, carboxylic acid results for core 12PL1 illustrate a much more minor proportion of terrestrial derived carboxylic acids ($C_{24:0}$ and $C_{26:0}$) as described by Meyers (2003). The shorter saturated carboxylic acids chains ($C_{16:0}$ and $C_{18:0}$) have been shown to represent aquatic organisms (Kawamura and Ishiwatari, 1981), but also a ubiquitous signal of all biota (Meyers, 2003). If the latter interpretation of Meyers (2003), that $C_{16:0}$ and $C_{18:0}$ represent components of all forms of life, is applied then the surprisingly large proportions of shorter-chained carboxylic acids may simply be a component of the surrounding terrestrial flora and explain this discrepancy. In general though carboxylic acids have been more useful as a tool for indicating the degree of organic matter recycling as they are much more sensitive to degradation, particularly the unsaturated acids, than their n-alkane counterparts (Meyers, 2003). The fact that unsaturated $C_{18:1}$ and $C_{22:1}$ are present in measurable amounts throughout core 12PL1 suggests that Pyramid Lake is not undergoing significant organic matter recycling or that the sediments are so young degradation has not yet altered their composition. This may also be supported by the lack of bacterial derived n-alkanes which typically signify more extensive degradation through microbial activity (Figure 3.4) (Meyers and Teranes, 2001). Diagenetic effects have been shown to confound carbon isotopic signatures and C/N ratios, however, due to the lack of diagenetic evidence in these sediment cores proxies should represent other conditions such as past rates of primary productivity and

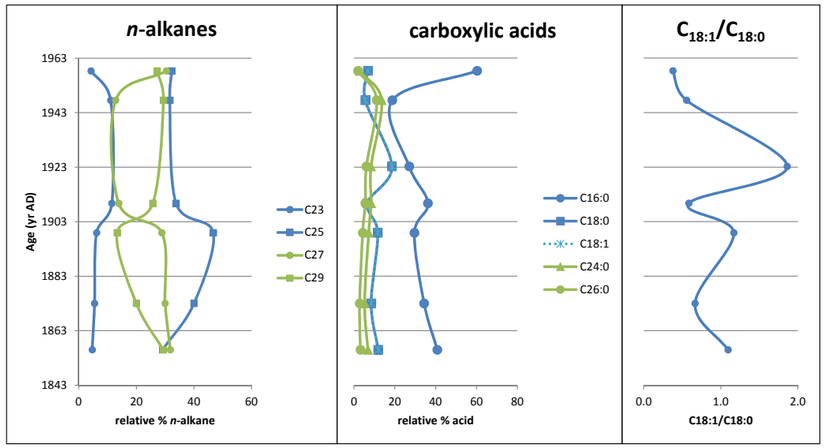

Figure 4.6: Relative proportions of n-alkanes (left, blue = aquatic plants, green = terrestrial plants) and saturated carboxylic acids (middle, blue = algal/general biota signature, dotted blue = algal, green = terrestrial) versus age in years AD for core 12PL5. Ratios of unsaturated:saturated carboxylic acids (right) show relative changes in temperature as suggested by Kawamura and Ishiwatari (1981) with blue = cooling and red = warming.

organic matter provenance more accurately (Fogel and Cifuentes, 1993; Meyers and Lallier-Vergès, 1999; Meyers and Teranes, 2001).

Concentrations of carbon and $CaCO_3$ in organic matter rich sediments, defined as greater than 10 percent organic carbon, generally display an inverse relationship as a result of greater dissolution of $CaCO_3$ (Dean, 1999). Higher concentrations of organic matter can lower the pH of lake water due to the decomposition of accumulating organic matter and organic acids, ultimately resulting in greater dissolution of calcium carbonate (Dean, 1999). Since percent total carbon levels were mostly within the definition of organic-rich matter defined by Dean (1999) for both cores, one would suspect this inverse relationship between percent carbon and percent calcium carbonate assuming the total carbon is predominately organic (Figures 4.4 and 4.5). Simply by examining the trends, this inverse relationship only seems apparent for core 12PL5 (Figure 4.5). By plotting percent carbon and calcium carbonate against each other, core 12PL5 exhibits a much stronger inverse correlation with an R^2 value of 0.4478 while core 12PL1 shows an R^2 value of 0.0165 signifying little to no relationship (Figure 4.7). The lack of an inverse relationship seen in core 12PL1 may suggest different diagenetic and/or sediment deposition processes between the two sub-basins in Pyramid Lake or error associated with decalcification. Therefore, core 12PL1's credibility is suspect as biogenic silica results utilized these decalcified sample masses. For all of these reasons, core 12PL5, which illustrates a much stronger inverse correlation between carbon and calcium carbonate, will be focused upon for past primary productivity interpretations.

Paleoproductivity

Biogenic silica is generally a strong indicator for past rates of primary productivity (Conley, 1988; Conley and Schelske, 2001). Increased (decreased) percentages of biogenic silica produced in the frustule's of diatoms correlates to increase (decrease) abundances of primary producers and, therefore, it may serve as a proxy for primary productivity which may be stimulated or dampened by nutrient dynamics (Conley and Schelske, 2001). The relative changes exhibited by percent biogenic silica in core 12PL5 display moderately high values at the bottom, decreasing to essentially 0 between 1855 and 1880 followed by a period of limited yet stable conditions through 1923 (Figure 4.4). At this point an increase in relative percentages begins and continues through the surface dated at 1961 (Figure 4.4). The relative changes seen in biogenic silica are mirrored by those of percent carbon and nitrogen, which are generally representative of relative concentrations of organic matter and at times productivity (Figure 4.4) (Meyers and Teranes, 2001). By strictly looking at biogenic silica and concentrations of organic matter, a strong argument can be made for a state of oligotrophication between 1855 and 1880, followed by limited primary productivity and a period of eutrophication from 1923 onward.

Past conditions of primary productivity may be teased apart with the use of carbon and nitrogen isotopic signatures; however, recent carbon isotope records must first be corrected for the Suess Effect, the gradual depletion in atmospheric CO2 by 1.4 ‰ since 1840 as a result of increased fossil fuel burning (Figure 1.13). Uncorrected $\delta^{13}C$ trends for both cores initially displayed overall depletion up core (Figures 3.2 and 3.3);

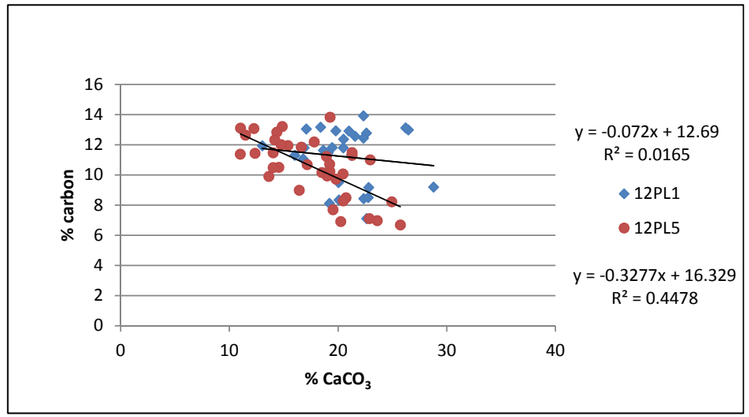

Figure 4.7: Percent carbon versus calcium carbonate ($CaCO_3$) for cores 12PL1 (red) and 12PL5 (blue) illustrating the degree of inverse correlation typically seen in organic matter-rich sediments suggested by Dean (1999).

however, after the correction model employed by Schelske and Hodell (1995) was applied, different trends became apparent (Figures 4.4 and 4.5). Corrected $\delta^{13}C$ for cores 12PL5 and 12PL1 display a variable, yet relatively consistent and unchanging trend up core which may be indicative of stable lake productivity as enrichment (depletion) would signify increasing (decreasing) primary productivity (Figures 4.4 and 4.5) (Brenner et al., 1999; Schelske and Hodell, 1995). If a lake is under conditions of low to moderate primary productivity, as indicated by biogenic silica concentrations in Pyramid Lake, algae are able to preferentially utilize lighter ^{12}C and, consequently, changes in paleoproductivity may not be seen in the carbon isotope record (Torres et al., 2012).

Carbon isotope signatures are also subject to temperature and diagenetic effects which may obscure primary productivity signals (Meyers and Lallier-Vergès, 1999). In terms of temperature the recent warming documented by NIWA (Figure 1.5) would cause an enrichment in $\delta^{13}C$ as a result of decreased fractionation (Fogel and Cifuentes, 1993) and since no significant enrichment trends are seen, temperature change is likely not reflected in stable isotopes (Figures 4.4 and 4.5). The presence of unsaturated carboxylic acids, which are particularly vulnerable to microbial degradation (Meyers, 2003), and lack of bacterial n-alkanes suggests low levels of organic matter recycling and microbial reworking of sediments (Figure 3.4). With this in mind, it becomes apparent that $\delta^{13}C$ is not particularly sensitive to changes in primary productivity and temperature in Pyramid Lake (Figures 4.4 and 4.5).

The slight enrichment seen in nitrogen isotopes up core may signify eutrophication as well, however, the use of $\delta^{15}N$ as a proxy for primary productivity is not nearly as reliable as $\delta^{13}C$ as it may be greatly altered by a number of processes within the nitrogen cycle (Figures 4.4 and 4.5) (Talbot, 2002). What $\delta^{15}N$ may signify is that the lake is rather pristine and not under the influence of anthropogenic perturbations such as fertilizers which would record a much more enriched $\delta^{15}N$ signature if organic and much more depleted signature if synthetic (Talbot, 2002). The fact that general $\delta^{13}C$ values are relatively depleted indicate carboxylation of dissolved CO_2 and not HCO_3^- which is synthesized during eutrophic or hypereutrophic conditions resulting in more enriched $\delta^{13}C$ signals up to 9 ‰ higher (Meyers and Lallier-Vergès, 1999). Nitrogen isotopes in conjunction with uptake of dissolved CO_2 and the lack of algal-derived C_{17} n-alkanes identified in core 12PL5 suggest that Pyramid Lake is under oligotrophic conditions with oligotrophication occurring from 1855 to 1880 and eutrophication beginning around 1923 as suggested by percent biogenic silica, carbon and nitrogen (Figures 4.4, 4.5 and 3.4) (Chikaraishi et al., 2004).

Twentieth Century Warming

The current global trend in twentieth century warming was preceded by the Little Ice Age (LIA), a global cooling event typically constrained between 1400 and 1850 AD (Shulmeister et al., 2004). In New Zealand, this period was associated with a poleward shift in the circumpolar wind belt, strengthening of westerly circulation and neoglaciation of Southern Alp glaciers terminating about 100 years before present deduced from moraine clusters and pollen records indicating stunted vegetation growth (Kirkbride and Winkler, 2012; Shulmeister et al., 2004). Changes in temperature have been shown to

positively correlate with rates of primary productivity and biogenic silica records (Elbert et al., 2013) such that the decrease in biogenic silica exhibited at the base of core 12PL5 from 1855 to 1880 may indicate the effects of global cooling associated with the tail-end of the LIA.

Considering recent trends in global warming and the published increase of New Zealand's mean air temperature by 1.0°C from 1855 to 2004 and by 0.4°C since 1950, it seemed reasonable to compare proxies against temperature trends. The ratio of unsaturated to saturated fatty acids has been employed as a temperature proxy based on the condition that organisms develop double bonds under cooler temperatures as a means to maintain membrane structure (Kawamura and Ishiwatari, 1981). With this in mind, a rough temperature proxy based on the eight samples from core 12PL5 shows relative variations in temperature throughout the core with a consistent warming trend beginning around 1923 and continuing through 1963 (Figure 4.8). This trend generally follows that of New Zealand's mean annual temperature; however, the decrease in temperatures from the carboxylic acid proxy seen from about 1910 to 1923 does not follow that of the mean annual temperatures reported by NIWA. This may be attributed to the fact that of the seven temperature sites incorporated into the temperature average, none were from the Fiordland region, with the closest being from Dunedin roughly 300 km away on the opposing side of the south island (Google Maps, 2012; NIWA, 2010). The distinctly rugged and varied orography of New Zealand's produces heterogeneous climates over short distances throughout the country such that NIWA's mean annual temperature series may not be accurately represented on shorter decadal time scales in vicinity of Pyramid Lake (Salinger and Mullan, 1999; Ummenhofer et al., 2009). Additionally, the carboxylic acid temperature proxy illustrates a contrasting episode of warming during the end of the LIA at the base of core 12PL5 (Figure 4.8). This "warming trend" may in fact be the result of organic matter degradation in the older sediments as they may have had sufficient time to begin this process compared to the younger sediments up core. Regardless, the hypothesized decrease in primary productivity in association with LIA global cooling must be interpreted with caution as the temperature proxies and trends seen here are either absent (NIWA) or do not follow (carboxylic acids).

Though there are shifts between relative cooling and warming exhibited by the ratio of unsaturated to saturated carboxylic acids, the overall recent trend in warming within the last century is clearly apparent through two temperature proxies and suggests that it may be a strong driver for increased primary productivity (Figure 4.8) (Elbert et al., 2013). Increasing temperatures have also been shown to induce more frequent El Nino years, the strongest regional driver in New Zealand climate variability (IPCC, 2007), resulting in precipitation levels up to 200 mm yr^{-1} greater in the Fiordland region of New Zealand, capable of delivering large proportions of allocthonous organic matter to Pyramid Lake (Figure 1.4) (Ummenhofer and England, 2007). Unfortunately, there were no precipitation proxies employed in this study, however, Salinger and Mullan (1999) have reported increasing precipitation throughout the last century which may account for greater concentrations of carbon and nitrogen as a result of increased terrestrial run-off and delivery of allochthonous organic matter (Figure 4.8). Additionally, the possibility exists that nitrogen availability increases as climate warms, accelerating soil mineralization and the delivery of nutrients to Pyramid Lake (Hobbie et al. 1999).

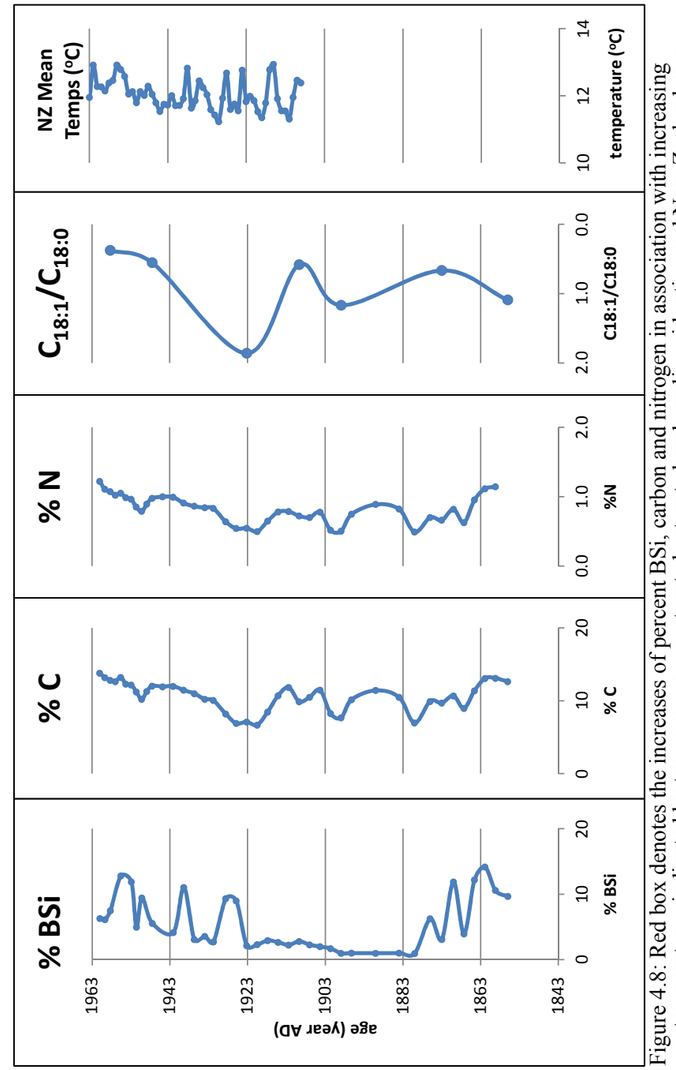

Figure 4.8: Red box denotes the increases of percent BSi, carbon and nitrogen in association with increasing temperatures indicated by two sources, unsaturated:saturated carboxylic acid ratios and New Zealand mean temperatures (NIWA), beginning around 1923 as inferred from the northern sub-basin (core 12PL5). The blue box possibly indicates the end of the Little Ice Age (note $C_{18:1}/C_{18:0}$ temperature proxy does not follow).

An influx of nutrients may stimulate primary productivity, represented by the increase of percent biogenic silica, carbon, nitrogen and enrichment of $\delta^{15}N$ near the surface of cores (Figures 4.4 and 4.5). However, it is not necessarily supported by C/N ratios as it would be expected for ratios to decrease more significantly with algal growth suggesting this may only be a portion of the story (Figures 4.4, 4.5 and 4.8) (Meyers and Teranes, 2001).

Another possible contributor to soil erosion exists in the local fauna of the region. Since New Zealand developed without the presence of terrestrial herbivores, native plant species are particularly vulnerable to grazing. The introduction of the red deer (Cervus elaphus) in the late 1800's to early 1900's may have initiated accelerated and sustained levels of soil erosion in the understory mountain beech forests. Red deer populations are now plentiful throughout the Fiordland region restricting the recovery of soil stability (Veblen and Stewart, 1982). Like erosion induced by increased precipitation C/N ratios are not fully supportive, and in general it is hard to say if and what the cause of increased erosion is based on lack of sufficient proxies, such as magnetic susceptibility and grain size, for these scenarios.

In addition to an increase in primary productivity, another strong possibility for the increase in organic matter proxies (percent carbon and nitrogen) and biogenic silica beginning around 1923 may lie in the large degree of seasonality associated with Pyramid Lake (Figure 4.8). Multiple visits to the field site by the University of Otago through winter and summer seasons revealed a seasonal lake level change of between 2 and 3 meters measured via moss lineations on rock features adjacent to the lake and physical observations along the shoreline (Figures 4.9 and 4.10, respectively) (Anderson, 2012). Considering that Pyramid Lake has no evident outlet streams, lake levels are particularly vulnerable to the effects of evaporation, which are exacerbated by the increasing temperatures reported by NIWA and interpreted through unsaturated:saturated carboxylic acid ratios (Figure 4.8). During winter months the lake is refilled following intensified precipitation of rain and snow and presumably contributes large proportion of terrestrial organic matter via run-off (Anderson, 2012; Jeng and Marshall, 2004). The high degree of seasonality and abnormally low lake level during summer months seen in Pyramid Lake translates to progressive resuspension and redistribution of littoral sediment to the deeper lakes basins. The relocation of sedimentary organic matter would effectively concentrate the sediments where both cores were obtained resulting in increasing percentages of carbon, nitrogen and biogenic silica (Figure 4.8) (Jellison et al, 1996). This scenario is only one of several possibilities including increased primary productivity and erosion starting around 1923 and like erosion, other supportive proxies are missing. As an example, mass accumulation rates (MAR) of carbon, expressed as mass of total organic carbon per unit of lake bottom area per unit of time, have been used to measure delivery rates and preservation of total organic carbon percentages (Jellison et al., 1996; Meyers, 2003). If MAR values were to be calculated for Pyramid Lake the validity of this specific scenario could be tested.

Figure 4.9: Moss lineations, marked by black arrows, observed on the shore of Pyramid Lake suggesting seasonal lake level changes of 2 to 3 meters, modified from Anderson (2012).

Figure 4.10: Pyramid Lake during March 2012 (left) and May 2012 at the time of coring (right). The photos exhibit the large degree of lake level variation through the seasons and the redistribution of littoral sediments when levels are low, from Anderson (2012).

Chapter 5: Conclusion

Conclusion

The geochemical records held within the sediments of Pyramid Lake suggest that temperature change has played a critical role in the developement of past conditions. Decreases in primary productivity from 1855 through 1880 may be linked to global cooling associated with the tail-end of the Little Ice Age, however, sufficient evidence from temperature proxies is missing. What can be suggested with more certainty are the developments which began around 1923 marked by consistent and uniform increases in percent biogenic silica, carbon, nitrogen. Coupled with temperature increase inferred from carboxylic acids and measured by New Zealand's National Institute of Water and Atmospheric Research (NIWA), 20th century global warming appears to be inducing eutrophication in Pyramid Lake. An additional explanation for the most recent rising trends is increasingly drastic seasonality causing enhanced littoral sediment redistribution to the lake basins. Despite recent eutrophication, Pyramid Lake appears to be under a consistent state of low productivity or oligotrophy. In terms of organic matter provenance, geochemical proxies suggest that it is predominantly vascular (terrestrial and/or aquatic derived) with minimal deposition of algae throughout the timeframe of 1855 through 1963.

Stable isotopes suggest that the watershed in which Pyramid Lake is situated is not under the direct influence of anthropogenic perturbations such as industry or agriculture during the measured timeframe. What is apparent is the increase in temperature, likely exacerbated by human-induced activity such as fossil fuel burning represented by the Suess Effect, and its influence on lake processes and dynamics. Though the age model excludes the developments of the latter half of the 20th century, it would not be far-fetched to assume eutrophication has continued. If warming trends are to continue into the future as predicted by the IPCC, Pyramid Lake's status could become eutrophic or even hypereutrophic which would issue in a host of other problems. With this being said, it is pertinent to pay close attention to the environmental and climatic developments within the Fiordland region of New Zealand in an effort to fully understand any additional and potentially unnatural and potentially damaging alterations to Pyramid Lake.

Future Work

One of the most significant holes found in this study was the lack of an accurate age model. An application of ^{210}Pb would rectify this issue as it is a function of radioactive decay rather than an increase in concentrations limited to a decade's length of time as in the case of $^{239+240}$Pu. With the sensitivity of surface sediments seen, it is easy to lose that critical timeframe during the 1960's to efficiently date sediments through plutonium. Additionally, core acquisition of the most recent lake sediments could shed light on the continuing effects of global climate change through the present. It may also give the opportunity to try and correlate changes within Pyramid Lake to documented shifts in atmospheric circulation patterns, related to SAM and ENSO, beginning in the middle of the 20th century.

In terms of paleoproductivity, biogenic silica procedures clearly had their faults and this study would benefit from reanalysis of this proxy to ensure past conditions of primary productivity are accurately represented. The addition of a stratigraphic log would add a sedimentological side to this project and help support and clear relative changes in erosion as contributors to geochemical changes seen in the record through grain size and physical appearances of sediment. Additionally, the issue of erosion could be clarified by a magnetic susceptibility record which would require an intact core to be run through a GeoTek scanner. Further isotopic work could inlcude δD records which may illustrate relative changes in aridity and humidity and δ^{13}C and δ^{15}N on the identified compound-specific lipids, shedding light on relative changes in the aquatic and terrestrial worlds in and around Pyramid Lake.

References

Anonymous, 2012, Alpine Fault: (http://www.gns.cri.nz/Home/Learning/Science-Topics/Earthquakes/Major-Faults-in-New-Zealand/Alpine-Fault10/23 2012).

Anonymous, 2012, Google Maps: (https://maps.google.com/10/25 2012).

Anonymous, 2012, Green Lake Track: (http://www.doc.govt.nz/parks-and-recreation/tracks-and-walks/fiordland/southern-fiordland/green-lake-track/10/22 2012).

Anonymous, 2012, Methods: Particulate Biogenic Silica: (http://nasl.cbl.umces.edu/Methods.htm).

Anonymous, 2010, 'Seven-station' series temperature data: (http://www.niwa.co.nz/our-science/climate/information-and-resources/nz-temp-record/seven-station-series-temperature-data.

Anderson, H., 2012, Modern sedimentary process and core analysis for the determination of sediment provenance of Pyramid Lake, Fiordland, New Zealand: p. 1 - 35.

Augustinus, P., Reid, M., Andersson, S., Deng, Y., and Horrocks, M., 2006, Biological and geochemical record of anthropogenic impacts in recent sediments from Lake Pupuke, Auckland City, New Zealand: Journal of Paleolimnology, v. 35, p. 789 - 805.

Brenner, M., Whitmore, T.J., Curtis, J.H., Hodell, D.A., and Schelske, C.L., 1999, Stable isotope (^{13}C and ^{15}N) signatures of sedimented organic matter as indicators of historic lake trophic state: Journal of Paleolimnology, v. 22, p. 205 - 221.

Cai, W., Shi, G., Cowan, T., Bi, D., and Ribbe, J., 2005, The response of the southern annular mode, the East Australian Current, and the southern mid-latitude ocean circulation to global warming: Geophysical Research Letters, v. 32.

Chikaraishi, Y., Naraoka, H., and Poulson, S.R., 2004, Hydrogen and carbon isotopic fractionations of lipid biosynthesis among terrestrial (C3, C4 and CAM) and aquatic plants: Phytochemistry, v. 68, p. 1369 - 1381.

Conley, D.J., 1988, Biogenic silica as an estimate of siliceous microfossil abundance in Great Lakes sediments: Biogeochemistry, v. 6, p. 161-179.

Conley, D.J., and Schelske, C.L., 2001, Biogenic Silica: Tracking Environmental Change using Lake Sediments, v. 1, p. 281 - 293.

Dean, W.E., 1999, The carbon cycle and biogeochemical dynamics in lake sediments: Journal of Paleolimnology, v. 21, p. 375-393.

Eggimen, D.W., Manheim, F.T., and and Betzer, P.R., 1980, Dissolution and analysis of amorphous silica in marine environments: Journal of Sedimentary Petrology, v. 50, p. 215 - 225.

Elbert, J., Wartenburger, R., von Gunten, L., Urrutia, R., Fischer, D., Fujak, M., Hamann, Y., Greber, N.D., and Grosjean, M., 2013, Late Holocene air temperature variability reconstructed from the sediments of Laguna Escondida, Patagonia, Chile (45°30'S): Palaeogeography, Palaeoclimatology, Palaeoecology, v. 369, p. 482 - 492.

Filippelli, G.M., 2008, The global phosphorus cycle: past, present and future: Elements, v. 4, p. 89 - 95.

Fogel, M., L., and Cifuentes, L.A., 1993, Isotope Fractionation during Primary Production, *in* Engel, M.H. and Macko, S.A., eds., Organic Geochemistry: Principles and Applications: New York, NY, Plenum Press, p. 73 - 98.

Francey, R., Allison, C., Etheridge, D., Trudinger, C., Enting, I., Leuenberger, M., Langenfelds, R., Michel, E., and Steele, L., 1999, A 1000-year high precision record of $\delta^{13}C$ in atmospheric CO_2: Tellus, v. 51, p. 170 - 193.

Friedli, H., Lötscher, H., Oeschger, H., and Siegenthaler, U., 1986, Ice core record of the $^{13}C/^{12}C$ ratio of atmospheric CO_2 in the past two centuries: Nature, p. 237–238.

Hancox, G.T., and Perrin, N.D., 2009, Green Lake Landslide and other giant and very large postglacial landslides in Fiordland, New Zealand: Quaternary Science Reviews, v. 28, p. 1020-1036.

Hennessy, K., Fitzharris, B., Bates, B.C., Harvey, N., Howden, S.M., Hughes, L., Salinger, J., and Warrick, R., 2007, Australia and New Zealand, *in* Parry, M.L., Canziani, O.F., Palutikof, J.P., van der Linden, P.J. and Hanson, C.E., eds., Climate Change 2007: Impacts, Adaption and Vulnerability. Contribution of Working Group II to the Fourth Assessment Report of the Intergovernmental Panel on Climate Change: Cambridge, UK, Cambridge University Press, p. 507 - 540.

Heyng, A.M., Mayr, C., Lücke, A., Striewski, B., Wastegård, S., and Wissel, H., 2012, Environmental changes in northern New Zealand since the Middle Holocene inferred from stable isotope records ($\delta^{15}N$, $\delta^{13}C$) of Lake Pupuke: Journal of Paleolimnology, p. 351 - 366.

Hobbie, E.A., Macko, S.A., and Shugart, H.H., 1999, Interpretation of nitrogen isotope signatures using the NIFTE model: Oecologia, v. 120, p. 404 - 415.

Jellison, R., Anderson, R.F., Melack, J.M., and Heil, D., 1996, Organic matter accumulation in sediments of hypersaline Mono Lake during a period of changing salinity: Limnology and Oceanography, v. 41, p. 1536 - 1544.

Kawamura, K., and Ishiwatari, R., 1981, Polyunsaturated fatty acids in a lacustrine sediment as a possible indicator of paleoclimate: Geochimica Et Cosmochimica Acta, v. 45, p. 149 - 155.

Keeling, C., D., Piper, S.C., Bacastow, R., B., Wahlen, M., Whorf, T.P., Heimann, M., and Meijer, H.A., 2001, Exchanges of atmospheric CO_2 and $^{13}CO_2$ with the terrestrial biosphere and oceans from 1978 to 2000: Scripps Institution of Oceanography Reference, v. 1, p. 1 - 22.

Ketterer, M.E., and Szechenyi, S.C., 2008, Determination of plutonium and other transuranic elements by inductively coupled plasma mass spectrometry: A historical perspective and new frontiers in the environmental sciences: Spectrochimica Acta Part B, v. 63, p. 719 - 737.

Kirkbride, M.P., and Winkler, S., 2012, Correlation of Late Quaternary moraines: impact of climate variability, glacier response, and chronological resolution: Quaternary Science Reviews, v. 46, p. 1 - 29.

Langenfelds, R.L., Francey, R.J., Pak, B.C., Steele, L.P., Lloyd, J., Trudinger, C.M., and Allison, C.E., 2002, Interannual growth rate variations of atmospheric CO_2 and its $D^{13}C,H_2$, CH_4, and CO between 1992 and 1999 linked to biomass burning: Global Biogeochemical Cycles, v. 16, p. 1 - 22.

Leinen, M., 1977, A normative calculation technique for determining opal in deep-sea sediments: Geochimica Cosmochimica Acta, v. 41, p. 671 - 676.

Leng, M.J., and Marshall, J.D., 2004, Paleoclimate interpretation of stable isotope data from lake sediment archives: Quaternary Science Reviews, v. 23, p. 811 - 831.

Mark, A.F., and Dickinson, K.J.M., 2001, *Deschampsia cespitosa* subalpine tussockland on the Green Lake landslide, Hunter Mountains, Fiord Ecological Region, New Zealand: New Zealand Journal of Botany, v. 39, p. 577 - 585.

Mark, A.F., Rawson, G., and Wilson, J.B., 1979, Vegetation pattern of lowland raised eastern Fiordland, New Zealand: New Zealand Journal of Ecology, v. 2, p. 1 - 10.

McGlone, M.S., 1989, The Polynesian settlement of New Zealand in relation to environmental and biotic changes: New Zealand Journal of Ecology, v. 12, p. 115 - 129.

McWethy, D.B., Whitlock, C., Wilmshurst, J.M., McGlone, M.S., and Li, X., 2009, Rapid deforestation of South Island, New Zealand, by early Polynesian fires: The Holo cene, v. 19, p. 883-897.

Meyers, P.A., 2003, Applications of organic geochemistry to paleolimnological reconstructions: a summary of examples from the Laurentian Great Lakes: Organic Geochemistry, v. 34, p. 261 - 289.

Meyers, P.A., and Lallier-Vergès, E., 1999, Lacustrine sedimentary organic matter records of Late Quaternary paleoclimates: Journal of Paleolimnology, v. 21, p. 345 - 372.

Meyers, P.A., and Teranes, J.L., 2001, Sediment organic matter: Tracking Environmental Change using Lake Sediments, v. 2, p. 239-269.

Mortlock, R.A., and and Froelich, P.N., 1989, A simple method for the rapid determination of biogenic opal in pelagic marine sediments: Deep-Sea Research, v. 36, p. 1415 - 1426.

Newnham, R., McGlone, M., Moar, N., Wilmshurst, J., and Vandergoes, M., 2012, The vegetation cover of New Zealand at the Last Glacial Maximum: Quaternary Science Reviews, p. 1 - 13.

Page, M.L., Trustrum, N.A., Orpin, A.R., Carter, L., Gomez, B., Cochran, U.A., Mildenhall, D.C., Rogers, K.M., Brackley, H.L., Palmer, A.S., and Northcote, L., 2010, Storm frequency and magnitude in response to Holocene climate variability, Lake Tutira, North-Eastern New Zealand: Marine Geology, p. 30 - 44.

Parsons, T.R., Maita, Y., and Lalli, C.M., 1984, A Manual of Chemical and Biological Methods for Seawater Analysis: New York, Pergamon Press, p. 25 - 28.

Peterson, B.T., and Fry, B., 1987, Stable isotopes in ecosystem studies: Annual Review of Ecology and Systematics, v. 18, p. 293-320.

Peterson, B.J., and Howarth, R.W., 1987, Sulfur, carbon and nitrogen isotopes used to trace organic matter flow in the salt-marsh estuaries of Sapelo Island, Georgia: Limnol ogy and Oceanography, v. 32, p. 1195 - 1213.

Pierrou, U., 1976, The global phosphorus cycle: Ecological Bulletins, v. 22, p. 75 - 88.

Pilskaln, C.H., Silver, M.W., Davis, D.L., Murphy, K.M., Lowder, S.A., Gritton, B.R. and Lews, L.A., 1991, Technical Report No. 92-9. Laboratory Techniques for the Handling and Geochemical Analysis of Water Column Particulate and Surface Sediment Samples. March 1992. Monterey Bay Aquarium Research Institute.

Rump, L.R., Kasting, J.F., and Crane, R.G., 2004, Chapter 15: Short-Term Climate Variabilty, *in* The Earth System: Upper River Saddle, New Jersey, Pearson Education, Inc., p. 289 - 316.

Salinger, M.J., and Griffiths, G.M., 2001, Trends in New Zealand daily temperature and rainfall extremes: International Journal of Climatology, v. 21, p. 1437 - 1452.

Salinger, M.J., and Mullan, A.B., 1999, New Zealand climate: temperature and precipitation variations and their links with atmospheric circulation 1930 - 1994: International Journal of Climatology, v. 19, p. 1049 - 1071.

Sauer, P.E., Eglinton, T.L., Hayes, J.M., Schimmelmann, A., and Sessions, A.L., 2001, Compound-specific D/H ratios of lipid biomarkers from sediments as a proxy for environmental and climatic conditions: Geochimica Et Cosmochimica Acta, v. 65, p. 213 - 222.

Schelske, C.L., Conley, D.J., Stoermer, E.F., Newberry, T.L., and Campbell, C.D., 1986, Biogenic silica and phosphorus accumulation in sediments as indices of eutrophica tion in the Laurentian Great Lakes: Hydrobiologia, v. 143, p. 79-86.

Schelske, C.L., and Hodell, D.A., 1995, Using carbon isotopes of bulk sedimentary organic matter to reconstruct the history of nutrient loading and eutrophication in Lake Erie: Limnology and Oceanography, v. 40, p. 918-929.

Sharp, Z., 2007, Carbon in the Low-Temperate Environment, *in* Principles of Stable Isotope Geochemistry: Upper Saddle River, NJ, Pearson Education, Inc., p. 149 -178.

Shulmeister, J., Goodwin, I., Renwick, J., Harle, K., Armand, L., McGlone, M.S., Cook, E., Dodson, J., Hesse, P.P., Mayewski, P., and Curran, M., 2004, The Southern Hemi sphere westerlies in the Australasian sector over the last glacial cycle: a synthesis: Quaternary International, v. 118 - 119, p. 23 - 53.

Striewski, B., Mayr, C., Flenley, J., Naumann, R., Turner, G., and Lücke, A., 2009, Multi-proxy evidence of late Holocene human-induced environmental changes at Lake Pupuke, Auckland (New Zealand): Quaternary International, p. 69 - 93.

Talbot, M.R., 2002, Nitrogen isotopes in paleolimnology: Tracking Environmental Change using Lake Sediments, v. 2, p. 401-439.

Torres, I.C., Inglett, P.W., Brenner, M., Kenney, W.F., and Reddy, K.R., 2012, Stable isotope ($\delta^{13}C$ and $\delta^{15}N$) values of sediment organic matter in subtropical lakes of different trophic status: Journal of Paleolimnology, v. 47, p. 693 - 706.

Ummenhofer, C.C., and England, M.H., 2007, Interannual extremes in New Zealand precipitation linked to modes of southern hemisphere climate variability: Journal of Climate, v. 20, p. 5418-5440.

Ummenhofer, C.C., Sen Gupta, A., and England, M.H., 2009, Causes of late twentieth-century trends in New Zealand precipitation: Journal of Climate, v. 22, p. 3 - 19.

Veblen, T.T., and Stewart, G.H., 1982, The effects of introduced wild animals on New Zealand forests: Annals - Association of American Geographers, v. 72, p. 372 - 397.

Verburg, P., 2007, The need to correct for the Suess Effect in the application of $\delta^{13}C$ in sediment of autotrophic Lake Tanganyika, as a productivity proxy in the Anthropocene: Journal of Paleolimnology, v. 37, p. 591 - 602.

Welicky, K., Suess, E., Ungerer, C.A., Muller, P.J., and and Fischer, K., 1983, Problems with accurate carbon measurements in marine sediments and particulate matter in seawater: Limnology and Oceanography, v. 28, p. 1252 - 1259.

Wetzel, R.G., 2001, Limnology: lake and river ecosystems: Sand Diego, Academic Press.